treatment difference with a power of 0.85 and a 1-sided alpha of 0.025, 190 patients per group will be needed. However, because we plan to perform two interim analyses, we will need 193 patients per group [17]. Taking into account several patients dropping out, the total sample size to be recruited will be 200 patients in each treatment group, i.e., 600 patients will be recruited in this study.

Interim analysis

There will be two formal interim analyses on the safety and efficacy of the primary end point: after 198 and 396 randomized patients are enrolled and followed up for 6 months. For the interim analyses on efficacy, the DSMB will evaluate the primary end point using the Lan-DeMets method with the O'Brien-Fleming spending function. Asymmetric stopping boundaries are planned, with early termination of the study recommended in the event of evidence of overwhelming benefit (2-sided $P<.001$ favoring EPO) or substantive harm (2-sided $P<.01$ against EPO) once sufficient events have accrued.

Statistical analysis

Data will be analyzed based on an intention-to-treat principle. The efficacy end point is LVEF improvement. The null hypothesis, that all treatment groups will have the same mean LVEF improvement, will be tested against the alternative hypothesis, that the mean LVEF improvement in the treatment groups will increase in the order of placebo, EPO (6,000 IU) and EPO (12,000 IU), according to the contrast test with a contrast coefficient (−1, 0, 1) based on the t-statistic. The contrast test will be evaluated based on a 1-sided significance level of 0.025. The secondary efficacy end point of OS in each group will be analyzed by the Kaplan-Meier method and compared using the log-rank test. Cardiovascular events and NT-ProBNP at the 6-months follow-up will be analyzed by a nonparametric test (e.g., Wilcoxon rank sum test). Safety analyses will be performed to summarize the adverse events in each treatment group. The baseline characteristics of the study patients will be summarized using frequencies and percentages for categorical variables and using means with standard deviations for continuous variables.

Current status

EPO-AMI-II began enrolling patients in December 2011. As of May 15, 2012, the application for the Evaluation System of Investigational Medical Care is ongoing, and 14 of 24 eligible centers have been approved. Completion of study enrollment is targeted for September 30, 2014. Allowing for the 6-month follow-up of the final randomized patient, trial completion is anticipated by March 2015.

Discussion

We have started the EPO-AMI-II study to clarify the safety and efficacy of low-dose EPO in the improvement of LVEF in STEMI patients with a low LVEF (<50 %). EPO-AMI-II is a multicenter, prospective, randomized, double-blind, placebo-controlled, dose-finding study in patients with their first STEMI.

Randomized clinical studies to clarify the effects of low-dose EPO in patients with STEMI

Therapies that can reduce myocardial damage and augment neovascularization in the heart after an MI may be beneficial in patients with STEMI. Experimental studies demonstrate that the intravenous administration of EPO at the onset of reperfusion reduces myocardial infarct size and prevents cardiac reverse remodeling, with enhanced neovascularization in the heart after an MI [6, 7]. Recently, proof-of-concept studies using high-dose EPO have reported inconsistent cardioprotection results from EPO in patients with STEMI (Table 3). The use of high-dose EPO at the time of reperfusion for an acute MI to salvage the myocardium or to improve LV function will not be further pursued in any newly initiated study.

In contrast, low-dose EPO is likely to be cardioprotective in small clinical trials [11–13]. Potential mechanisms to explain the dose-dependent discrepancy of EPO in cardioprotection may be attributable to platelet activation and the existence of an optimal dose for limiting infarct size. Platelet activation by a high dose of EPO [14] and the existence of an optimal dose for limiting infarct size [15] may explain the dose-dependent discrepancy of EPO-induced cardioprotection. Because EPO has structural similarity with thrombopoietin, high-dose EPO increases platelet production and reactivity, which leads to an increased risk of thrombosis and cardiovascular events. Additionally, a dose response curve of the bioactivity of cytokines does not necessarily appear to be guided by a sigmoid function. Positive intracellular signal of cytokine receptors via serial chain reaction of protein tyrosine kinases is typically interfered by automated circuit reaction of protein tyrosine phosphatase such as SHP1 to avoid overdoing of growth and inflammation [18]. In fact, administration of high-dose EPO lost its cardioprotective activity in rat and mouse coronary ischemia/reperfusion models [15, 19]. The rationale for EPO treatment for

Table 3 Overview of randomized controlled studies investigating the effects of EPO in patients with acute myocardial infarction

Trial	Dose of EPO	Primary outcome	Result	Cardiovascular event
REVIVAL-3	33,333 IU×3 (0, 24, 48 h)	LV EF	No change	Increase (not significant)
HEBE-III	60,000 IU	Infarction size	No change	Decrease (significant)
REVEAL	60,000 IU	Infarction size	No change	Increase (not significant)
EPOC-AMI	6,000 IU×3 (day 0, 2, 4)	LV EF	Improve	No change
EPO-AMI-I	12,000 IU	LV EF	Improve	No change
EPO-AMI-II	6,000 or 12,000 IU	LV EF		

patients with STEMI lies in the low-dose EPO trials, although these have only been small clinical trials to date.

Protocol of EPO-AMI-II study

On the basis of a post-hoc analysis of our pilot study (EPO-AMI-I) and a recent proposal from workshops [20–22], we have modified the protocol for the EPO-AMI-II study. First, we created new inclusion criteria to include patients with an LVEF <50 %. Only patients who have large myocardial infarcts can receive benefits from any adjunctive therapy [23, 24]. Consistently, the post-hoc analysis of the EPO-AMI-I study revealed that STEMI patients with an LVEF <50 % received large benefits from EPO administration11 (Fig. 1). When patients with significant stenotic lesions in non-infarct-related arteries that required revascularization were excluded, more than 90 % of STEMI patients who met the inclusion and exclusion criteria presented with a proximal left anterior descending artery in the EPO-AMI-I study. This type of STEMI patient will receive more benefit from adjunctive therapy [23, 24]. Second, we have shortened the therapeutic time window from the onset of chest pain to reperfusion time (from 24 h to 12 h), which will also result in a shorter time window between EPO administration and the onset of chest pain. For example, in rats with a permanent coronary occlusion, EPO does not effectively reduce myocardial infarct size when administered ≥24 h after the MI [25]. These protocol modifications of the EPO-AMI-I study will improve the efficacy and safety of low-dose EPO in patients with STEMI.

Safety of EPO in STEMI patients

In the EPO-AMI-I (12,000 IU) and EPOC studies (6,000 IU × 3) in which low-dose EPO was administered, the risk of cardiovascular events was not increased [11, 12]. When high-dose EPO was administered, the results were inconsistent. In the REVEAL study, the subanalysis showed that EPO (60,000 IU) had a higher incidence of serious adverse events, although the authors noted that the analysis was based on a very small number of events. Conversely, in the HEBEIII study, the subanalysis revealed that EPO showed a trend toward a reduction of enzymatic infarct size and significantly reduced the incidence of the combined endpoint (cardiovascular death, myocardial infarction, in-stent thrombosis, unstable angina and heart failure). In the REVIVAL study, EPO (33,000 IU × 3) showed a trend toward an increased rate of serious adverse effects. Their meta-analysis showed that the administration of EPO appeared to be safe for patients with acute STEMI [26]. For the safety of patients in the EPO-AMI-II study, a report system for serious adverse events has been established, and the clinical research coordinator will often visit the hospitals that participate in this study. Recently, the post-hoc analysis suggested the association of high-dose EPO with the restenosis of the culprit lesion, although no significant differences in late lumen loss between the EPO and placebo groups were observed [27, 28]. Additionally, no significant difference in late lumen loss was found when low-dose EPO was used [11, 12].

Quantification of LV function and infarct size

In the EPO-AMI-II study, we are only including patients with a first STEMI because ECG-gated SPECT allows for no distinction between previous and new infarcts. The primary end point of this study is to evaluate the improvement of LVEF between the acute and chronic stages (Table 2). In the chronic stage, ECG-gated SPECT with adenosine allows for the evaluation of the residual myocardial ischemia. One alternative evaluation method is cardiac magnetic resonance imaging, which may be able to assess the at-risk area and the final infarct size, but this technique remains to be validated for quantification [29].

Conclusions

Because the randomized control trials conducted to date have used high-dose EPO and demonstrated heterogeneous results, the EPO-AMI-II study will clarify the safety and efficacy of low-dose EPO in STEMI patients with LV dysfunction in double-blind, placebo-controlled, multicenter studies (Appendix).

Acknowledgments We sincerely thank Drs. Akira Myoi and Yasutaka Hayashida (Medical Center for Translational Research Osaka University Hospital) and Dr. Yoichi Yamamoto (Center for Clinical Investigation and Research, Osaka University Hospital) for advice on conducting the EPO-AMI-II study. We also thank Dr. Hiroyuki Uesaka for statistical aspects of the study design. We thank Hiromi Umezome, Sakiko Ichijo (Center for Clinical Investigation and Research, Osaka University Hospital) for their assistants and Sugako Mitsuoka for her excellent secretarial work. The management of this study is supported by Grants-in-Aid from the Ministry of Health, Labour and Welfare of Japan, a Japanese Circulation Society Grant for Translational Research 2010 and the Support and Training Program for Translational Research at Osaka University.

Discloures None.

Appendix

Principle Investigators:

Aizawa Y, Komuro I.

Steering Committee:

Higo S, Ito H, Kato K, Kobayashi N, Ozawa T, Minamino T, Suzuki H. Tobaru T, Toba K.

Data Management:

Higo S, Takahara S (Medical Center for Translational Research Osaka University Hospital, Suita, Japan)

Statistical Analysis:

Yamamoto K, Hamasaki T (Department of Biomedical Statistics, Osaka University Graduate School of Medicine, Suita, Japan)

SPECT Core Center:

Ishida Y (Kansai Rosai Hospital Cardiovascular Center, Amagasaki, Japan), Sakata Y, (Department of Cardiovascular Medicine, Osaka University Graduate School of Medicine, Suita, Japan), Yoshimura N (Department of Radiology, Niigata University Medical and Dental Hospital, Niigata, Japan)

Data and Safety Monitoring Board:

Fujio Y (Laboratory of Clinical Science and Biomedicine, Graduate School of Pharmaceutical Sciences, Osaka University, Japan), Hasegawa S (Department of Cardiology, Osaka Kosei Nenkin Hospital, Osaka, Japan), Seki Y (Department of Internal Medicine (Hematology), Niigata Prefectural Shibata Hospital, Japan). Sugimoto T (Department of Mathematical Sciences, Hirosaki University Graduate School of Science and Technology, Japan)

EPO-AMI-II Investigators:

Chiba-Nishi General Hospital, Chiba, Japan.
Yoshida T, Kuramochi M
Dokkyo University School of Medicine, Tochigi, Japan;
Ishimitsu T, Kobayashi N
Fujisawa City Hospital, Fujisawa, Japan
Yano H, Himeno H
Higashi-Osaka City General Hospital, Osaka, Japan
Kijima Y, Ichikawa M
Kansai Rosai Hospital, Amagasaki, Japan;
Uematsu M, Watanabe T
Kanto Rosai Hospital, Kawasaki, Japan
Namiki A, Shibata M
Kokura Memorial Hospital, Kitakyushu, Japan
Yokoi H, Nomura A
National Cerebral and Cardiovascular Center, Suita, Japan
Yasuda S, Kotani J
Niigata University Medical and Dental Hospital, Niigata, Japan;
Toba K, Ozawa T
Nippon Medical School, Tokyo, Japan
Mizuno K, Yasutake M
Nozaki Tokushukai Hospital, Osaka, Japan
Okutsu M, Sumitsuji S
Okayama University Graduate School of Medicine, Dentistry and Pharmaceutical Sciences, Okayama, Japan;
Ito H, Kusano K
Osaka General Medical Center, Osaka, Japan;
Fukunami M, Yamada T
Osaka National Hospital, Osaka, Japan;
Yasumura Y, Hirooka K
Osaka Police Hospital, Osaka, Japan;
Ueda Y, Hirata A
Osaka Rosai Hospital, Sakai, Osaka, Japan;
Nishino M, Makino N
Osaka University Graduate School of Medicine, Suita, Japan;
Komuro I, Minamino T
Sakakibara Heart Institute, Fuchu, Japan
Tobaru T, Asano R
Senri Critical Care Medical Center, Osaka Saiseikai Senri Hospital, Suita, Japan
Ito N, Doi, Y
Shonan Kamakura General Hospital, Kamakura, Japan
Saito S, Tobita K
Showa University Fujigaoka Hospital, Yokohama, Japan;
Suzuki H, Wakabayashi K
Showa University School of Medicine, Tokyo, Japan
Kobayashi Y, Koba S
St. Marianna University School of Medicine, Kawasaki, Japan
Yoneyama Y, Akashi Y
Tachikawa General Hospital, Nagaoka, Niigata, Japan;
Aizawa Y, Sato M

References

1. Lloyd-Jones D, Adams RJ, Brown TM, et al. Executive summary: heart disease and stroke statistics–2010 update: a report from the American Heart Association. Circulation. 2010;121:948–54.

2. Takii T, Yasuda S, Takahashi J, et al. Trends in acute myocardial infarction incidence and mortality over 30 years in Japan: report from the MIYAGI-AMI Registry Study. Circ J. 2010;74:93–100.
3. Sutton MG, Sharpe N. Left ventricular remodeling after myocardial infarction: pathophysiology and therapy. Circulation. 2000;101:2981–8.
4. Minamino T. Cardioprotection from ischemia/reperfusion injury: basic and translational research. Circ J. 2012;76:1074–82.
5. Jelkmann W. Erythropoietin: structure, control of production, and function. Physiol Rev. 1992;72:449–89.
6. Hirata A, Minamino T, Asanuma H, et al. Erythropoietin just before reperfusion reduces both lethal arrhythmias and infarct size via the phosphatidylinositol-3 kinase-dependent pathway in canine hearts. Cardiovasc Drugs Ther. 2005;19:33–40.
7. Hirata A, Minamino T, Asanuma H, et al. Erythropoietin enhances neovascularization of ischemic myocardium and improves left ventricular dysfunction after myocardial infarction in dogs. J Am Coll Cardiol. 2006;48:176–84.
8. Ott I, Schulz S, Mehilli J, et al. Erythropoietin in patients with acute ST-segment elevation myocardial infarction undergoing primary percutaneous coronary intervention: a randomized, double-blind trial. Circ Cardiovasc Interv. 2010;3:408–13.
9. Voors AA, Belonje AM, Zijlstra F, et al. A single dose of erythropoietin in ST-elevation myocardial infarction. Eur Heart J. 2010;31:2593–600.
10. Najjar SS, Rao SV, Melloni C, et al. Intravenous erythropoietin in patients with ST-segment elevation myocardial infarction: REVEAL: a randomized controlled trial. JAMA. 2011;305:1863–72.
11. Ozawa T, Toba K, Suzuki H, et al. Single-dose intravenous administration of recombinant human erythropoietin is a promising treatment for patients with acute myocardial infarction—randomized controlled pilot trial of EPO/AMI-1 study. Circ J. 2010;74:1415–23.
12. Taniguchi N, Nakamura T, Sawada T, et al. Erythropoietin prevention trial of coronary restenosis and cardiac remodeling after ST-elevated acute myocardial infarction (EPOC-AMI): a pilot, randomized, placebo-controlled study. Circ J. 2010;74:2365–71.
13. Opie LH. Erythropoietin as a cardioprotective agent: down but not out. Heart. 2011;97:1537–9.
14. Vaziri ND. Thrombocytosis in EPO-treated dialysis patients may be mediated by EPO rather than iron deficiency. Am J Kidney Dis. 2009;53:733–6.
15. Baker JE, Kozik D, Hsu AK, Fu X, Tweddell JS, Gross GJ. Darbepoetin alfa protects the rat heart against infarction: dose–response, phase of action, and mechanisms. J Cardiovasc Pharmacol. 2007;49:337–45.
16. Uesaka H. A personal view of methods of sample size estimation for a clinical trial. Jpn J Biom. 2003;24:17–41.
17. Jennison C, Turnbull BW. Group sequential methods with applications to clinical trials. Boca Raton: Chapman & Hall/CRC; 2000.
18. Zhang J, Somani AK, Siminovitch KA. Roles of the SHP-1 tyrosine phosphatase in the negative regulation of cell signalling. Semin Immunol. 2000;12:361–78.
19. Kanellakis P, Pomilio G, Agrotis A, et al. Darbepoetin-mediated cardioprotection after myocardial infarction involves multiple mechanisms independent of erythropoietin receptor-common beta-chain heteroreceptor. Br J Pharmacol. 2010;160:2085–96.
20. Hausenloy DJ, Baxter G, Bell R, et al. Translating novel strategies for cardioprotection: the Hatter Workshop Recommendations. Basic Res Cardiol. 2010;105:677–86.
21. Schwartz Longacre L, Kloner RA, Arai AE, et al. New horizons in cardioprotection: recommendations from the 2010 National Heart, Lung, and Blood Institute Workshop. Circulation. 2011;124:1172–9.
22. Downey JM, Cohen MV. Why do we still not have cardioprotective drugs? Circ J. 2009;73:1171–7.
23. Piot C, Croisille P, Staat P, et al. Effect of cyclosporine on reperfusion injury in acute myocardial infarction. N Engl J Med. 2008;359:473–81.
24. Botker HE, Kharbanda R, Schmidt MR, et al. Remote ischaemic conditioning before hospital admission, as a complement to angioplasty, and effect on myocardial salvage in patients with acute myocardial infarction: a randomised trial. Lancet. 2010;375:727–34.
25. Moon C, Krawczyk M, Paik D, Lakatta EG, Talan MI. Cardioprotection by recombinant human erythropoietin following acute experimental myocardial infarction: dose response and therapeutic window. Cardiovasc Drugs Ther. 2005;19:243–50.
26. Li J, Xu H, Gao Q, Wen Y. Effect of erythropoiesis-stimulating agents in acute ST-segment elevation myocardial infarction: a systematic review. Eur J Clin Pharmacol. 2011;68:469–77.
27. Stein A, Mohr F, Laux M, et al. Erythropoietin-induced progenitor cell mobilisation in patients with acute ST-segment-elevation myocardial infarction and restenosis. Thromb Haemost. 2012;107:769–74.
28. Minamino T, Toba K, Higo S, Nakatani D, Ozawa T. Erythropoietin, progenitor cells and restenosis. A critique of Stein et al. Thromb Haemost. 2012;107:1193.
29. Carlsson M, Ubachs JF, Hedstrom E, Heiberg E, Jovinge S, Arheden H. Myocardium at risk after acute infarction in humans on cardiac magnetic resonance: quantitative assessment during follow-up and validation with single-photon emission computed tomography. JACC Cardiovasc Imaging. 2009;2:569–76.

Circulation Journal
Official Journal of the Japanese Circulation Society
http://www.j-circ.or.jp

Myocardial Layer-Specific Effect of Myoblast Cell-Sheet Implantation Evaluated by Tissue Strain Imaging

Yasuhiro Shudo, MD; Shigeru Miyagawa, MD, PhD; Satoshi Nakatani, MD, PhD; Satsuki Fukushima, MD, PhD; Taichi Sakaguchi, MD, PhD; Atsuhiro Saito, PhD; Toshihiko Asanuma, MD, PhD; Naomasa Kawaguchi, PhD; Nariaki Matsuura, MD, PhD; Tatsuya Shimizu, MD, PhD; Teruo Okano, PhD; Yoshiki Sawa, MD, PhD

Background: The implantation of skeletal myoblast (SMB) cell-sheets over the damaged area of a myocardial infarction (MI) has been shown to improve global left ventricular (LV) function through a paracrine effect. However, the regeneration process has not been fully evaluated. We hypothesized that the use of tissue Doppler strain M-mode imaging to assess myocardial layer-specific strain might enable detailed visual evaluation of the regenerative ability of SMBs.

Methods and Results: SMBs were cultured on temperature-responsive culture dishes to generate cell-sheets. At 4 weeks after inducing anterior MI, the animals were divided into 2 groups: SMB cell-sheet implantation and sham operation (n=6 in each). A total of 30 cell-sheets (1.5×10^7 cells/sheet) were placed on the epicardium, covering the infarct and border regions. Subendocardial and subepicardial strain values were measured in the infarct, border, and remote regions by tissue Doppler strain analysis. SMB cell-sheet implantation produced the following major effects: progression of LV remodeling was prevented and global LV ejection fraction increased; the subendocardial strain was significantly greater than the subepicardial strain in the treated border region; vascular density in the subendocardium was significantly higher than in the subepicardium in the treated region; the expression of vascular endothelial growth factor was significantly increased.

Conclusions: Tissue Doppler strain analysis allows precise evaluation of the effect of cell-sheet implantation on layer-specific myocardial function.

Key Words: Cytokines; Heart failure; Strain; Tissue Doppler

Heart failure still occurs frequently and is life-threatening, despite recent medical and surgical advances. Myocardial regenerative therapy is attracting growing interest as a means of improving left ventricular (LV) function in advanced heart failure.[1–3] However, recent clinical trials reported slightly disappointing results for cell transplantation by needle injection.[2–4] The major drawbacks of cell transplantation using that technique are poor retention and survival of the injected cells, local myocardial damage and potential lethal arrhythmias. The cell-sheet technique was developed to deliver cells efficiently without damaging the myocardium and, consequently, more effectively improve cardiac function than the needle injection method.[5–9] This therapeutic modality is already being used in the clinical setting.[10] It has been suggested that implantation of a skeletal myoblast (SMB) cell-sheet reverses LV remodeling via paracrine effects in which angiogenic factors constitutively released from the implanted cell-sheets induce neo-angiogenesis, increased vascular density and blood flow, thereby reversing hybernating myocardium.[5–10] However, detailed evaluation of functional improvement (eg, region-specific functional recovery associated with secreted cytokines) has not been performed. Moreover, the existing evidence base remains inconsistent, and the underlying mechanism and optimal protocols are still being debated.[11]

Tissue strain M-mode imaging based on the tissue Doppler technique (TDI-Q, Toshiba) was developed to accurately mea-

Received May 24, 2012; revised manuscript received October 15, 2012; accepted November 20, 2012; released online December 29, 2012 Time for primary review: 24 days

Department of Cardiovascular Surgery (Y. Shudo, S.M., S.F., T. Sakaguchi, A.S., Y. Sawa), Department of Health Sciences, Division of Functional Diagnostics (S.N., T.A.), Department of Pathology (N.K., N.M.), Osaka University Graduate School of Medicine, Suita; and Advanced Biomedical Engineer and Science, Tokyo Women's Medical University, Tokyo (T. Shimizu, T.O.), Japan

Presented at the American College of Cardiology's 60th Annual Scientific Session, ACCF/Herman K. Gold Young Investigator's Award in Molecular and Cellular Cardiology, New Orleans, LA, April 2–5, 2011.

Mailing address: Yoshiki Sawa, MD, PhD, Department of Cardiovascular Surgery, Osaka University Graduate School of Medicine, 2-15 Yamada-oka, Suita 565-0871, Japan. E-mail: sawa-p@surg1.med.osaka-u.ac.jp

ISSN-1346-9843 doi:10.1253/circj.CJ-12-0615

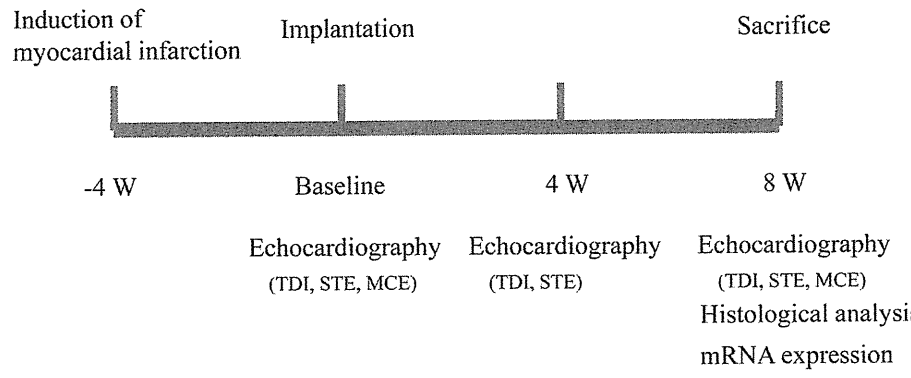

Figure 1. Study protocol for the assessment of cardiac function and histological analysis. TDI, tissue Doppler imaging; STE, speckle tracking echocardiography; MCE, myocardial contrast echocardiography.

sure myocardial layer-specific strain values, based on the transmural myocardial strain profile (TMSP).[12–14] Within the myocardium, the specific characteristics of each myocardial layer confer a different ability to improve regional myocardial performance.[15] We hypothesized that the myocardial layer-specific strain values might enable an assessment of regional functional improvement, based on the paracrine effects of cytokines following cell-sheet implantation. To investigate our hypothesis, we assessed the TMSP in a porcine model of myocardial infarction (MI).

Methods

Ethics

All studies were performed with the approval of the Ethics Committee of Osaka University. Humane animal care was used in compliance with the "Principles of Laboratory Animal Care" formulated by the National Society for Medical Research and the "Guide for the Care and Use of Laboratory Animals" prepared by the Institute of Animal Resources and published by the National Institutes of Health (Publication No 85-23, revised 1996). All authors had full access to the data and take full responsibility for its integrity. All authors have read and agreed to the manuscript as written. All procedures and evaluations, including the assessment of cardiac parameters, were carried out in a blinded manner.

Animal Models and Study Protocol (Figure 1)

We used 20 female mini-pigs (8–10 months old, 20–25 kg; Japan Farm Co Ltd, Kagoshima, Japan). They were anesthetized with intravenous ketamine (6 mg/kg) and sodium pentobarbital (10 mg/kg) for endotracheal intubation and then maintained with inhaled sevoflurane (1–2%). The pericardial space was exposed by left thoracotomy through the 4th intercostal space. The distal portion of the left anterior descending coronary artery (LAD) was directly ligated, followed by placement of an ameroid constrictor around the LAD just distal of the branching of the left circumflex coronary artery (LCX) to prevent sudden cardiac death from lethal ventricular arrhythmia and intolerance of ischemia.[5,16] This technique produces an MI model that has clinical relevance and can be used for appropriate preclinical studies with minimal procedure-related mortality (6 (30%) of the 20 mini-pigs died within 48 h of surgery primarily from acute cardiac failure).

Computer-generated random allocation generated 2 randomized study groups at 1 week after the induction of MI, and autologous cells were then isolated and grown in culture for 3 weeks for implantation. At 4 weeks after MI induction, the mini-pigs were again placed under general anesthesia for echocardiography followed by either cell-sheet implantation or sham operation. Two mini-pigs in which the LV ejection fraction (LVEF) was >40%, measured by transthoracic echocardiography using the Simpson's method before the treatment, were excluded from the study. At 4 and 8 weeks after either cell-sheet implantation or sham operation, the mini-pigs were again placed under general anesthesia for echocardiography examination. The mini-pigs were killed humanely following the 8-week echocardiography study for histological and biochemical analysis of the heart tissue.

Preparing and Grafting Skeletal Myoblast Cell Sheets

Autologous skeletal muscle weighing approximately 10–15 g was removed from the quadriceps femoris muscle, and purified autologous SMB cells were cultured for 3 weeks in preparation for implantation as described previously.[5] The cells were incubated in 60-mm temperature-responsive culture dishes (UpCell®; Cellseed, Tokyo, Japan) at 37°C for 24 h, with the cell numbers adjusted to 1.5×10^7 cells/dish. The dishes were then transferred to another incubator set at 20°C for 1 h to release the cultured cells as intact cell-sheets. SMB spontaneously detached to generate free-floating monolayer cell-sheets.

At 4 weeks after MI induction, the mini-pigs were randomly divided into the 2 treatment groups (n=6 in each): SMB cell-sheet implantation (Sheet group) or sham operation (Sham group). In the Sheet group, 30 cell-sheets (1.5×10^7 cells/sheet) with the total cell number being 4.5×10^8 were implanted on the epicardium of the ischemic area (LAD region) via median sternotomy approach under general anesthesia. Cell sheets were attached and fixed to the epicardial surface by stitching around the edge of the sheet.

Conventional Echocardiography

Global cardiac function was assessed using a commercially available echocardiograph machine with a 4.0-MHz transducer (Aplio; Toshiba, Otawara, Japan) before, and 4 and 8 weeks after cell-sheet implantation. Echocardiographic measurements included LV end-diastolic and end-systolic volumes (LVEDV

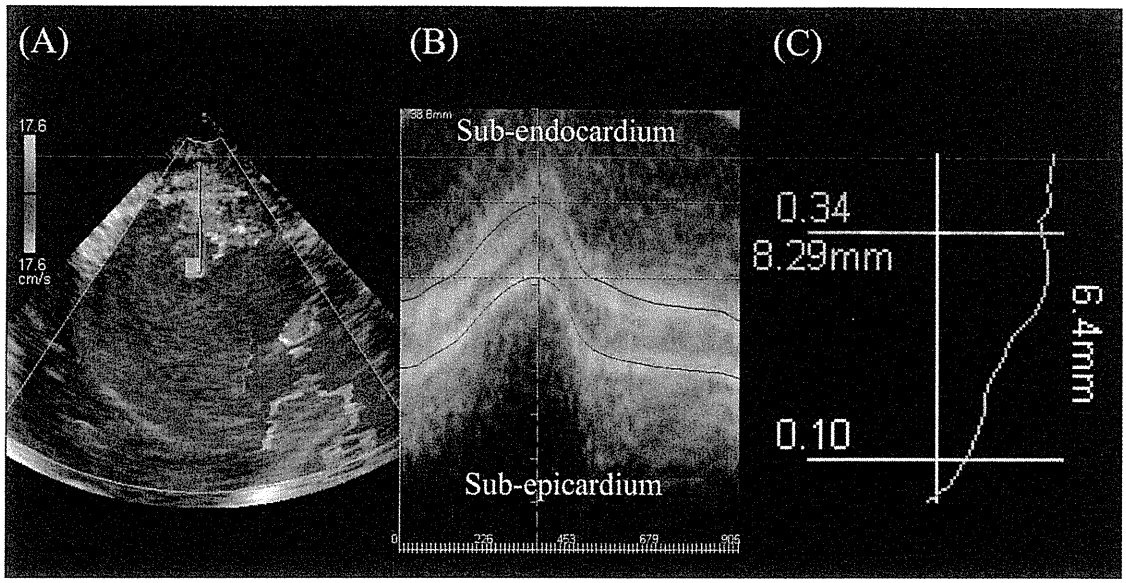

Figure 2. Measurement of transmural myocardial strain profile by tissue strain M-mode imaging and the indicated analysis software. (A) Recordings stored in the form of digital loops of 2 cardiac cycles for subsequent offline analysis. (B) LV endocardium and epicardium traced from an end-systolic frame. (C) Endocardial and epicardial borders automatically tracked through 1 cardiac cycle using analysis software (TDI-Q; Toshiba, Tokyo, Japan).

and LVESV, respectively), and LVEF, calculated as:

$$EF\ (\%) = 100 \times (LVEDV - LVESV) / (LVEDV).$$

Myocardial Layer-Specific Strain Using Tissue Doppler Strain M-Mode Imaging

Tissue strain M-mode imaging (frame rate, 82–118 frames/s) based on the tissue Doppler technique and the corresponding analysis software (TDI-Q, Toshiba, Otawara, Japan) were used to assess myocardial layer-specific strain. Parasternal short-axis images were recorded at the level of base, mid-ventricle, and apex by tissue Doppler imaging (Figure 2A). To obtain a strain image, TDI-Q first calculates the myocardial displacement of all pixels of tissue by integrating myocardial velocity over a certain period. Next, strain is obtained by evaluating the change in the distance between pairs of points defined on all pixels of the image by utilizing the displacement values. The initial time frame is set at end-diastole to evaluate myocardial deformation occurring in systole. To measure local strain accurately, it is essential to accurately obtain local velocity. Therefore, the present imaging system used tissue Doppler tracking and angle-correction techniques. Tissue Doppler tracking is an automatic motion tracking technique based on tissue Doppler information. By integrating the velocity of an index point on the ventricular wall, identified from tissue Doppler imaging, we could obtain myocardial displacement and predict where the index point would move next. By repeating this procedure, the system can automatically track the motion of the index point (Figure 2B). With this technique, the influence of myocardial translation can be ignored. The angle-correction technique enables Doppler incident angle dependency to be partially overcome. To correct the Doppler incident angle, a contraction center is set at the center of the LV cavity at end-systole in the short-axis view. The software automatically calculates the tissue velocity toward the contraction center (V motion) by dividing the velocity toward a transducer (V beam) by the cosine of the angle (θ) between the Doppler beam and the direction to the contraction center as follows:

$$V\ motion = V\ beam / \cos\theta$$

Using these 2 techniques, the software TDI-Q automatically cancelled the effect of myocardial translation and angle dependency, accurately assessing myocardial velocity, displacement, and strain. In previously described experiments, the displacement data obtained by this method correlated with true displacement.[17] Myocardial radial strain distribution over the myocardium is obtained as M-mode color-coded images and the profile of distribution (TMSP) at end-systole is shown as in Figure 2C. We divided the myocardium into subendocardial and subepicardial half-layers by the mid-point of the myocardium at end-systole. Mean strain values in the subendocardial half-layer and in the subepicardial half-layer were calculated by averaging the strain values over each layer in the infarcted (center of segment 13), border (edge of segment 7),[18] and remote regions (center of segment 10). In this study, the "infarcted" region was assigned predominantly to territories of the LAD, and the "remote" region was assigned to the LCX or right coronary artery.

Histological and Immunohistochemical Analyses

At 8 weeks after the treatment, the hearts were dissected and embedded in optimum cutting temperature compound, snap-frozen in liquid nitrogen, and cut into sections. The 5-μm-thick, paraffin-embedded sections fixed in 4% paraformaldehyde were stained with hematoxylin-eosin (HE) or Masson's trichrome. Using Image J software, the infarcted area was expressed as a percentage calculated as the positively stained LV area/total LV area in sections stained with Masson's trichrome. The 5-μm thick cryosections fixed in 4% paraformaldehyde were immunofluorolabeled with anti-von Willebrand factor

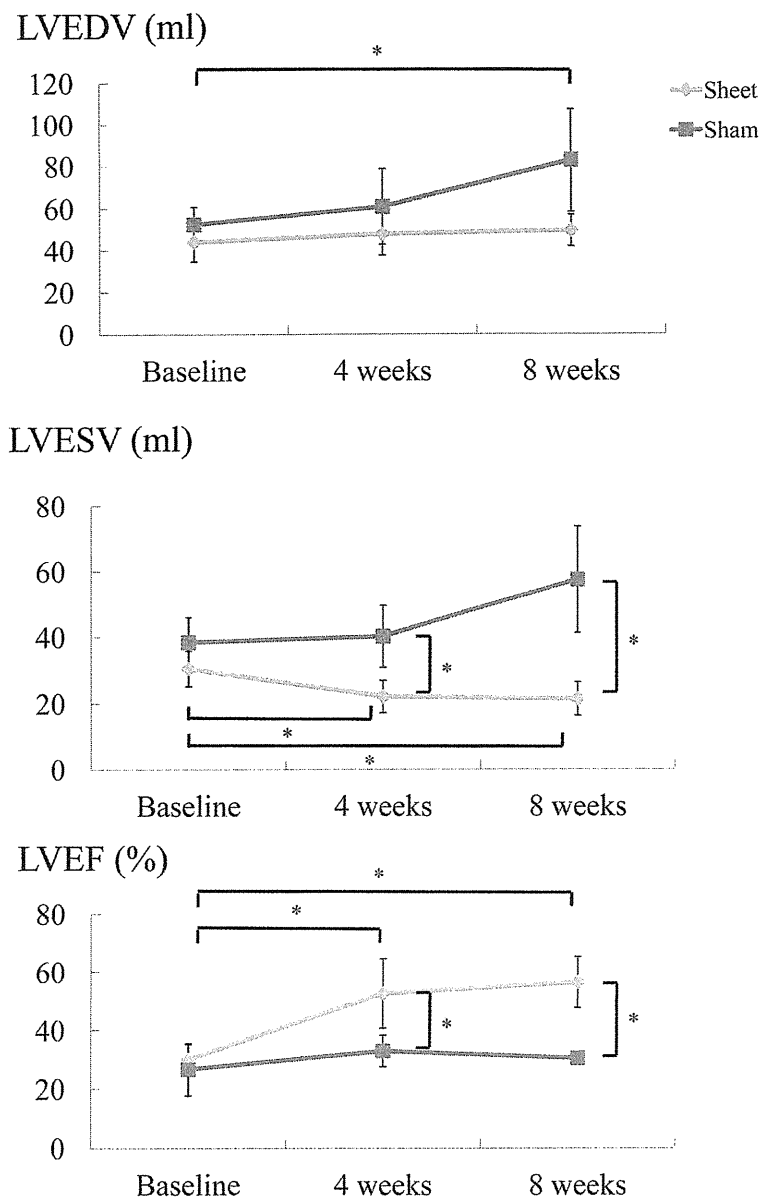

Figure 3. Echocardiographic analysis. LVEDV increased significantly at 8 weeks in the Sham group compared with baseline, and remained unchanged in the Sheet group. LVESV significantly decreased in the Sheet group at 4 and 8 weeks after implantation, showing a significantly lower value than that in the Sham group. LVEF significantly increased in the Sheet group at 4 and 8 weeks after implantation, showing a significantly higher value than that in the Sham group. n=6 in each group; *P<0.05. LVEDV, left ventricular end-diastolic volume; LVESV, left ventricular end-systolic volume; LVEF, left ventricular ejection fraction.

(vWF) antibody (1:250 dilution, Dako, Glostrup, Denmark). The numbers of capillary vessels that were positively stained and 5–10 μm in diameter in the subendocardium and subepicardium of the infarcted, border, and remote regions, in 10 individual, randomly selected fields per heart were counted under high-power magnification (×200) of a BioZero laser scanning microscope (Keyence, Osaka, Japan), then averaged to express vascular density (per mm^2).

Analysis of mRNA Expression

Total RNA was extracted from the border region of cardiac muscle tissue and reverse transcribed into cDNA using TaqMan Reverse Transcription Reagents (Applied Biosystems, Foster City, CA, USA). Real-time polymerase chain reaction (PCR) was performed for vascular endothelial growth factor (VEGF), basic fibroblast growth factor (bFGF), brain natriuretic peptide (BNP), intercellular adhesion molecule-1, tumor necrosis factor-α (TNF-α), interleukin-6 (IL-6), signal transducer and activator of transcription 3, and insulin-like growth factor-1 (IGF-1) using an ABI PRISM 7700 machine.[19] The average copy number of gene transcripts for each sample was normalized to that for GAPDH.

Statistical Analysis

SPSS software (version 11.0, Chicago, IL, USA) was used for statistical analyses. Continuous values are expressed as the mean (standard deviation). The significance of differences was determined using a 2-tailed multiple t-test with Bonferroni correction following repeated measures analysis of variance for individual differences. P<0.05 was considered statistically significant.

Results

Gradual Recovery of Global Systolic LV Function

Serial changes in global systolic and diastolic LV function after cell-sheet implantation were assessed by conventional echo-

Table. Hemodynamics and Strain Measurements

	SMB cell-sheet group (n=6)‡			Sham operation group (n=6)		
	Baseline	4 weeks	8 weeks	Baseline	4 weeks	8 weeks
Heart rate (beats/min)	64±12	66±10	62±13	62±14	62±9	66±14
Blood pressure						
Systolic (mmHg)	98±22	108±25	106±17	102±31	110±28	104±24
Diastolic (mmHg)	70±13	68±9	70±10	68±11	64±10	66±13
Conventional echocardiographic parameters						
End-diastolic volume (ml)	44.1±9.4	47.7±10.2	49.3±7.6	52.5±8.3	60.7±18.0	82.7±24.5*
End-systolic volume (ml)	30.6±5.3	22.1±4.9†,*	21.4±5.1†,*	38.5±7.4	40.2±9.3	57.4±16.2
Ejection fraction (%)	30.1±5.1	52.6±11.9†,*	56.4±8.8†,*	26.6±8.9	32.9±5.4	30.4±1.1
Transmural strain profile using tissue strain imaging						
Border region						
Subendocardial strain (%)	5.73±4.48	27.3±7.64†,*	39.5±8.32†,*	−0.96±1.96	−0.83±2.23	0.71±5.02
Subepicardial strain (%)	8.29±5.56	9.23±7.90	18.5±11.9	8.96±2.05	7.14±2.41	5.37±3.46
Infarct region						
Subendocardial strain (%)	2.77±1.97	6.64±7.90	4.93±4.63	−0.22±3.77	0.77±1.13	−0.21±2.18
Subepicardial strain (%)	−1.40±1.89	2.13±4.37	2.60±2.83	0.02±2.49	0.24±1.15	−0.10±1.07
Remote region						
Subendocardial strain (%)	67.6±17.6	69.2±21.6	75.1±14.3	59.0±4.36	51.8±7.46	46.8±8.29
Subepicardial strain (%)	35.5±12.3	43.3±17.9	53.8±6.91	38.3±8.12	39.9±8.28	35.9±5.47

†P<0.05 vs. Sham group, *P<0.05 vs. Baseline. ‡A total of 30 cell-sheets (1.5×10^7 cells/sheet) were placed on the epicardium, covering the infarct and border regions. SMB, skeletal myoblast.

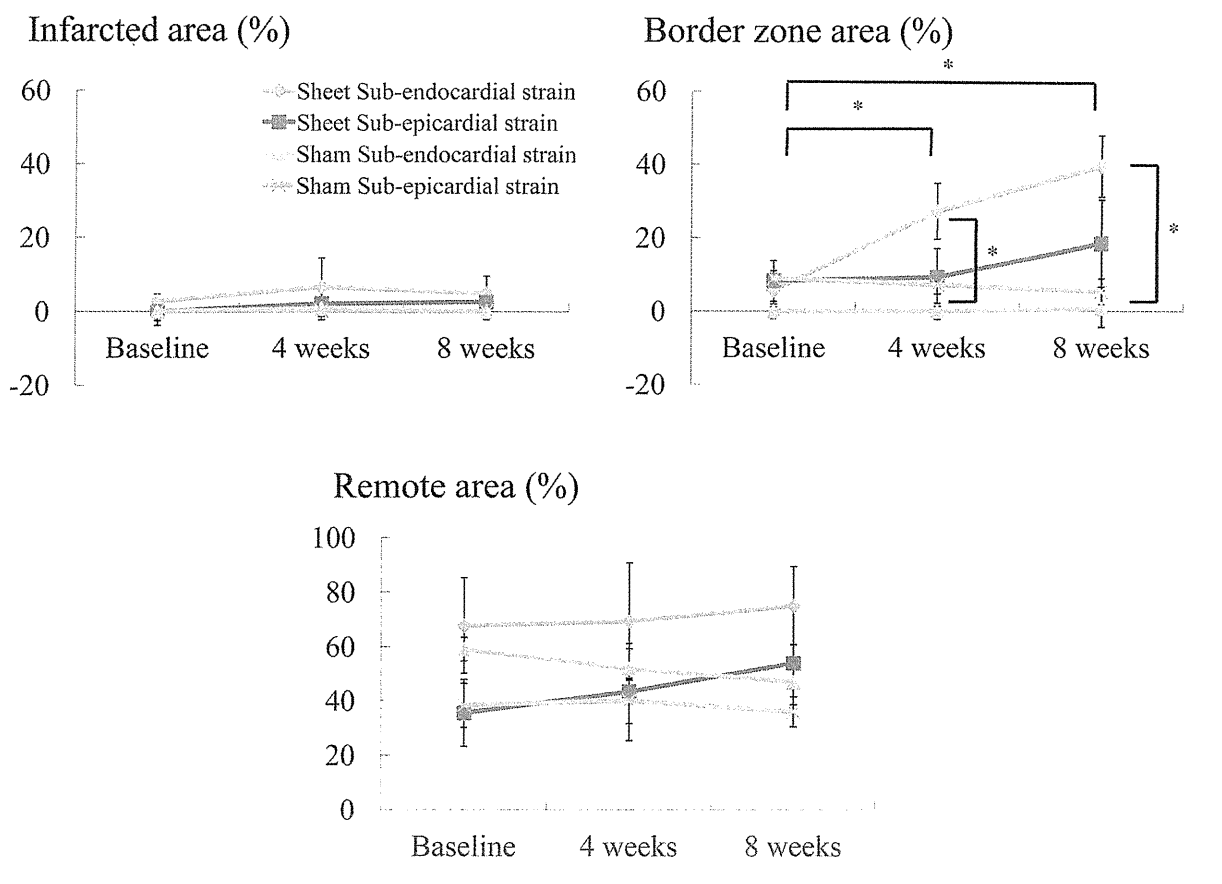

Figure 4. Myocardial layer strain value. In the treated border region, subendocardial strain significantly increased at 4 and 8 weeks after cell-sheet implantation, showing a significant increase in comparison with subepicardial strain. In the infarcted region, both subendocardial and subepicardial strain values were greater in the Sheet group than in the Sham group. In the remote region, no significant changes were observed. n=6 in each group; *P<0.05.

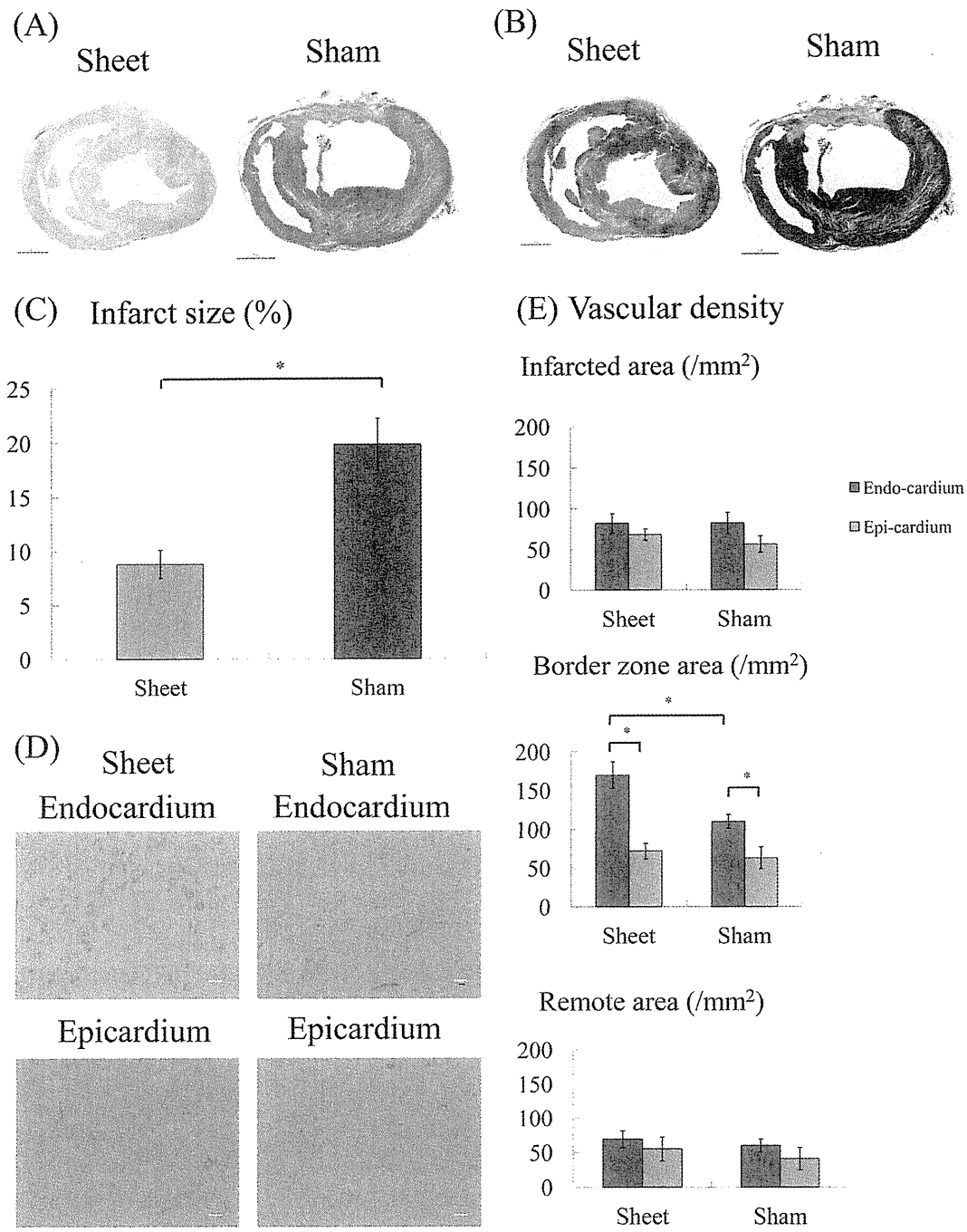

Figure 5. Histological findings. (A) Macroscopic (×40) view of the heart (HE). (B) Macroscopic (×40) views of the heart (Masson's trichrome). (C) The size of the infarcted area of the heart was significantly reduced in the Sheet group as compared with the Sham group. (D) Microscopic (×200) views of sections of the subendocardium and subepicardium in the treated border zone area stained with anti-von Willebrand factor (vWF) antibody (factor VIII) (bar=20 μm). (E) A greater number of vWF-positive blood vessels in the subendocardium compared with the subepicardium of the border zone area in the Sheet group. No significant changes are seen in the infarcted and remote areas. *P<0.05.

cardiography. Following sham operation, LVEDV and LVESV tended to increase till 8 weeks, while LVEF did not change significantly. In contrast, following SMB cell-sheet implantation, LVEDV did not change significantly, but LVESV significantly decreased and LVEF increased significantly at 4 and 8 weeks after SMB cell-sheet implantation compared with before the implantation. At 4 weeks after the treatment, LVESV was significantly smaller and LVEF was significantly greater in the Sheet group than in the Sham group, but there was no significant difference in LVEDV between them. At 8 weeks

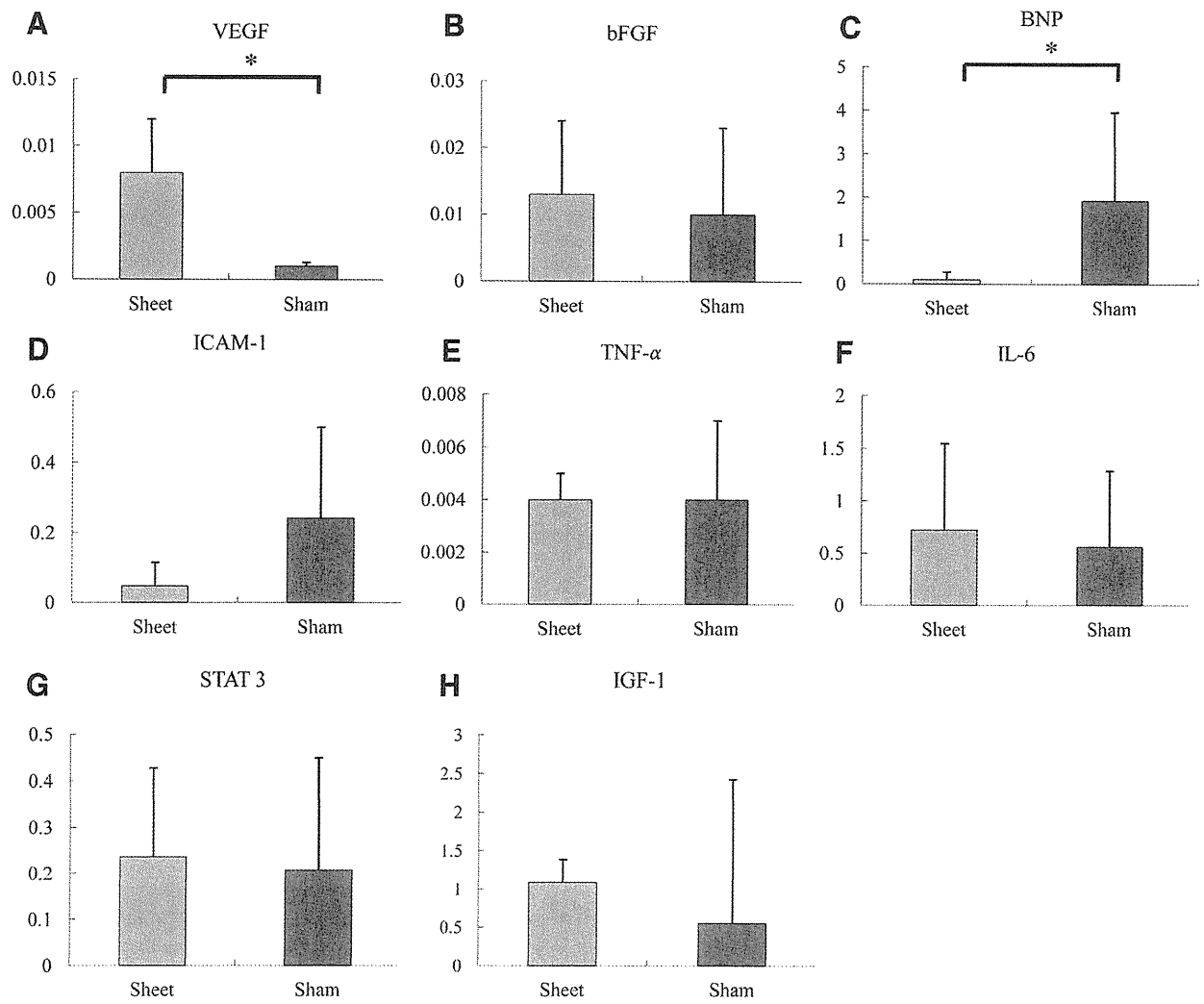

Figure 6. mRNA expression in cell-sheet implanted infarcted hearts determined by real-time PCR using porcine primers (A–H). VEGF mRNA expression was significantly increased in the Sheet group as compared with the Sham group. n=6 in each group; *P<0.05. PCR, polymerase chain reaction; VEGF, vascular endothelial growth factor.

after the treatment, both LVEDV and LVESV were significantly smaller and LVEF still greater in the Sheet group than in the Sham operation group (Figure 3, Table).

Myocardial Layer-Specific Recovery

Regional LV function in the infarct, border and remote areas was also examined in a myocardial-layer specific manner to assess the regional effects of SMB cell-sheet implantation in more detail by using the TMSP at 4 and 8 weeks post cell-sheet implantation (Figure 4, Table). Before the treatment, myocardial strain values of both the subendocardium and subepicardium were significantly smaller in the infarct and border areas compared with the remote area. After the sham operation, myocardial strain in both the subendocardium and subepicardium showed similar values for the infarct, border, and remote areas for 8 weeks. In contrast, subendocardial strain significantly increased at 4 and 8 weeks after cell-sheet implantation and was significantly larger than subepicardial strain in the treated border region. In the infarcted region, both subendocardial and subepicardial strain values tended to be greater in the Sheet group than in the Sham group. In the remote region, no significant changes were observed.

Modulation of Myocardial Structure

Myocardial structure, including fibrosis and vascularity, was assessed by HE staining, Masson's trichrome staining and immunohistochemistry for vWF at 8 weeks after the treatment (Figures 5A,B). The LV cavity was enlarged after the sham operation compared with after sheet implantation, and myocardial structure was well maintained post-sheet implantation compared with post-sham operation, as assessed by HE staining. Collagen had densely accumulated in the infarct area and was globally distributed in the remote area post-sham operation, whereas less collagen accumulated in either the infarct or remote area post-cell-sheet implantation compared with post-sham operation, as assessed by Masson's trichrome staining. The size of the infarcted area (ie, the percentage calculated as the positively stained LV area/total LV area), quantitatively

assessed by computer-based planimetry of Masson's trichrome-stained heart tissue, was significantly smaller in the Sheet group than in the Sham group (Figure 5C).

Vascular density, assessed by immunohistochemistry for vWF, in both the endocardium and epicardium, tended to be greater in the infarct and border areas than in the remote area of sham-operated hearts. In addition, vascular density in the endocardium was significantly greater than that in the epicardium in the border area post-sham operation, whereas vascular density did not differ significantly between the subendocardium and subepicardium in either the infarct or remote area of the sham-operated hearts. After cell-sheet implantation, vascular density did not differ between the subendocardium and subepicardium in either the infarct or remote area, but it was significantly greater in the subendocardium than in the subepicardium in the border region in the Sheet group. Only vascular density in the subendocardium of the border zone showed a significant difference between the sheet-implanted and sham-operated hearts (Figures 5D,E).

Profiles of Expression of Reverse LV Remodeling-Related Molecules

A variety of molecules that are expressed intramyocardial and potentially related to reverse LV remodeling were assessed by real-time PCR. Relative expression of VEGF was significantly increased in the Sheet group compared with the Sham group, whereas other factors, such as TNF-α, IL-6, bFGF and IGF-1, did not show any significant differences (Figure 6). Relative expression of BNP was significantly smaller post-cell-sheet implantation than post-sham operation.

Discussion

In the present study, SMB cell-sheet implantation produced the following major effects: (1) progression of LV remodeling was prevented and global LVEF decreased; (2) subendocardial strain was significantly greater than subepicardial strain in the treated border region; (3) vascular density in the subendocardium was significantly higher than in the subepicardium of the treated region; and (4) the expression of VEGF was significantly increased. Our data therefore suggest that SMB cell-sheet implantation enhanced the paracrine effect (eg, VEGF), inducing angiogenesis and thus improving regional myocardial performance in the targeted area, and these effects were more significant in the subendocardium than in the subepicardium of the border lesion.

The mechanism of restoration of damaged myocardium by SMB cell-sheet implantation is complex and many pathways are involved in the recovery of treated myocardium.[5–7,20,21] Recent reports have described the beneficial results of SMB cell-sheet implantation in several animal experimental models and patients with heart failure, which were primarily attributed to the following factors: the secretion of cytokines from the implanted cell-sheets (ie, paracrine effect), including angiogenic growth factors, the formation of capillary networks, and finally, mechanical inhibition of LV dilatation by implantation of cell-sheets.[1,3,5–10] Previous studies supported this and have shown that SMB and bone marrow-derived mesenchymal stem cell sheets secrete growth factors (eg, VEGF) into the myocardium, and that these factors accelerate neovascularization in the damaged area.[5–10] Among the many complex molecular and cellular mechanisms, the role of VEGF and its signaling pathway has been intensively investigated in vivo.[22] Toyota et al reported that the expression of VEGF is critical to the growth of coronary collateral vessels.[23] In the present study, VEGF expression was significantly increased in the Sheet group compared with the Sham group, suggesting that SMB cell-sheet implantation induced an angiogenic response via VEGF. Although many studies have proved that released cytokines from implanted cells play a major role in generating therapeutic effects on ischemic myocardium, there is currently no modality to precisely evaluate the section of damaged myocardium affected by released cytokines.

For tissue engineering as cardiac therapy, the creation of mature and functional vessels as neo-vascularization is essential. It has been reported that capillary formation occurs via 2 basic vessel-constructing processes: angiogenesis (ie, the formation of new capillaries via sprouting or intussusception from preexisting vessels), and vasculogenesis.[24] It has been also reported that angiogenesis requires dynamic temporal and spatial regulated interaction among endothelial cells, pericytes, and angiogenic factors.[25] Together with the morphology of vessels forming within myocardial tissues, including the diameter and stability of the vessel walls, we propose another possible mechanism that vessel maturation may occur under pathological stimuli such as increased blood perfusion in the in vivo environment.

To separately elucidate the effects of SMB cell-sheet implantation on LV regional function in the treated infarcted and border areas, we used tissue Doppler derived strain and the corresponding analysis software. SMB cell-sheet implantation therapy induced an improvement in regional myocardial performance in the treated border area, but not the treated infarcted area. Moreover, we speculate that regional functional recovery may correlate well with our data for the upregulation of VEGF gene expression and significant angiogenesis in the border region of the ischemic/infarcted myocardium. In addition, on the basis of the results of an improvement in the strain value as determined by tissue Doppler derived strain, the model used in the present study can be considered as the hibernating state, especially in the border region, instead of as a model of chronic MI.[15] Taken together, the results suggest that SMB cell-sheet therapy may rescue potentially salvageable myocardium partially by reperfusion, thus improving myocardial performance. Together with the paracrine effects of the implanted SMB cell-sheet, humoral substances might have a beneficial effect on native cardiomyocytes and viable surrounding muscle cells, leading to the prevention of global myocardial remodeling.[15] Our results may support the concept of a molecular mechanism of paracrine effect associated with cardioprotective factors released following SMB cell-sheet implantation.

The TMSP showed that SMB cell-sheet implantation induced a more significant regional recovery in the subendocardium than in the subepicardium, despite the SMB cell-sheet being implanted on the epicardium. To understand this mechanism in more detail, we performed tissue strain imaging and the results reflect the fundamental differences in functional properties within the LV myocardium. Ischemic injury did not occur in a uniform manner throughout the LV myocardium. Regional differences in metabolism and energy requirements render the endocardium more vulnerable to injury. Myocardial injury and stunning therefore usually originate in the endocardium and, with time, progress to include the epicardium.[26] In general, VEGF expression is activated under hypoxic conditions, a reasonable mechanism for holding oxygen tension constant.[27] Some previous investigators suggested that a soluble VEGF receptor (ie, sVEGFR1) increases in response to hypoxia.[28,29] It seems reasonable to assume that paracrine signaling between VEGF and sVEGFR1 might be evoked predominantly

in the ischemic region to regulate angiogenesis, and improve regional myocardial performance, in the face of hypoxia. Thus, the conceptual approach of SMB cell-sheet implantation is the eliciting of a cardiac protective response (eg, angiogenesis and microcirculation) during ischemia and prevention of the progression of ischemic injury and tissue necrosis. A possible mechanism to explain our results is that SMB cell-sheet implantation induces the release of cytokines and enhances the development of microvasculature (ie, microcirculation) that might be particularly vulnerable to injury during ischemia, and upon reperfusion, enhances the recovery of myocardial performance.[30] There is currently an emerging theory that the microcirculation could be the primary target for the amelioration of the potentially devastating consequences of ischemic injury. Nevertheless, it remains to be determined whether the primary benefits of SMB cell-sheet implantation are a consequence of (1) a cardioprotective effect by contributing directly to cardiomyocyte regeneration, (2) paracrine effects emanating from the SMB cell-sheet, or (3) a combination of these effects. Also, it is unclear whether the source of the therapeutic cytokines (eg, VEGF) is the implanted cells or native cardiac cells, such as ischemic cardiomyocytes, endothelial cells, or resident macrophages.

Study Limitations

Considerable caution must be exercised in extrapolating the present results. We did not validate myocardial strain values using other methods (eg, sonomicrometry). However, sonomicrometry is not always suitable for the assessment of transmural distribution of myocardial strain. We believe that our measurements were accurate because the displacement data obtained by our method were shown to be accurate.[31]

TDI is generally recognized as a 1D method and can measure myocardial deformation along the beam direction only. TDI-based strain estimation suffers from decorrelation caused by both axial motion and motion transverse to the beam direction. 2D speckle tracking strain imaging was introduced to overcome these limitations to myocardial imaging by estimating the 2D in-plane displacements with moderate frame rates.[32] These 2 methods are very different in principle and detail, directly affecting estimation accuracy, even of the same parameters. These differences must be noted when parameters from either method are applied clinically to myocardial contractility characterization. Moreover, the operator must avoid myocardium with large transverse motion to minimize the effect of transverse motion on TDI measurements.

Several investigators have suggested that a zone of dysfunctional myocardium caused by coronary artery occlusion might exist at the border of an infarct, with graded hypoperfusion extending out from the central region of infarction.[33,34] Subsequent reports demonstrated that coronary microvessels function essentially as end vessels with sharp boundaries between adjacent vascular beds, but that intermediate levels of mean blood flow can exist as a result of admixture of peninsulas of ischemic tissue intermingled with regions of normally perfused myocardium.[35–39] Although there is tremendous variability in the coronary artery blood supply to myocardial segments, it was believed to be appropriate to assign individual segments to specific coronary artery territories.

Conclusions

In conclusion, assessment of the TMSP enabled precise evaluation of the effect of cell-sheet implantation on layer-specific myocardial function. Autologous SMB cell-sheet implantation enhanced the paracrine effect, induced angiogenesis, and increased blood perfusion, thus improving regional myocardial performance more effectively in the subendocardium as compared with the subepicardium of the treated border zone area.

Sources of Funding

The present study was supported by Grants for the Research and Development of the Myocardial Regeneration Medicine Program from the New Energy Industrial Technology Development Organization (NEDO), Japan.

Acknowledgments

We thank Mr Shigeru Matsumi and Mrs Masako Yokoyama for their excellent technical assistance.

Disclosure

There is no conflict of interest related to this article.

References

1. Menasche P, Hagege AA, Scorsin M, Pouzet B, Desnos M, Duboc D, et al. Myoblast transplantation in heart failure. *Lancet* 2001; **357:** 279–280.
2. Ghostine S, Carrion C, Souza LC, Richard P, Bruneval P, Vilquin JT, et al. Long-term efficacy of myoblast transplantation on regional structure and function after myocardial infarction. *Circulation* 2002; **106:** I131–I136.
3. Hagege AA, Marolleau JP, Vilqiun JT, Alheritiere A, Peyrard S, Duboc D, et al. Skeletal myoblast transplantation in ischemic heart failure: Long-term follow-up of the first phase I cohort of patients. *Circulation* 2006; **114:** I108–I113.
4. Menasche P, Hagege AA, Vilquin JT, Desnos M, Abergel E, Pouzet B, et al. Autologous skeletal myoblast transplantation for severe postinfarction left ventricular dysfunction. *J Am Coll Cardiol* 2003; **41:** 1078–1083.
5. Miyagawa S, Saito A, Sakaguchi T, Yoshikawa Y, Yamauchi T, Imanishi Y, et al. Impaired myocardium regeneration with skeletal cell sheets: A preclinical trial for tissue-engineered regeneration therapy. *Transplantation* 2010; **90:** 364–372.
6. Miyagawa S, Sawa Y, Sakakida S, Taketani S, Kondoh H, Memon IA, et al. Tissue cardiomyoplasty using bioengineered contractile cardiomyocyte sheets to repair damaged myocardium: Their integration with recipient myocardium. *Transplantation* 2005; **80:** 1586–1595.
7. Memon IA, Sawa Y, Fukushima N, Matsumiya G, Miyagawa S, Taketani S, et al. Repair of impaired myocardium by means of implantation of engineered autologous myoblast sheets. *J Thorac Cardiovasc Surg* 2009; **130:** 646–653.
8. Sekiya N, Matsumiya G, Miyagawa S, Saito A, Shimizu T, Okano T, et al. Layered implantation of myoblast sheets attenuates adverse cardiac remodeling of the infarcted heart. *J Thorac Cardiovasc Surg* 2009; **138:** 985–993.
9. Miyagawa S, Roth M, Saito A, Sawa Y, Kostin S. Tissue-engineered cardiac constructs for cardiac repair. *Ann Thorac Surg* 2011; **91:** 320–329.
10. Fujita T, Sakaguchi T, Miyagawa S, Saito A, Sekiya N, Izutani H, et al. Clinical impact of combined transplantation of autologous skeletal myoblasts and bone marrow mononuclear cells in patients with severely deteriorated ischemic cardiomyopathy. *Surg Today* 2011; **41:** 1029–1036.
11. Janseens S, Dubois C, Bogaert J, Theunissen K, Deroose C, Desmet W, et al. Autologous bone marrow-derived stem-cell transfer in patients with ST-segment elevation myocardial infarction: Double-blind, randomized controlled trial. *Lancet* 2006; **367:** 113–121.
12. Maruo T, Nakatani S, Jin Y, Uemura K, Sugimachi M, Ueda-Ishibashi H, et al. Evaluation of transmural distribution of viable muscle by myocardial strain profile and dobutamine stress echocardiography. *Am J Physiol Heart Circ Physiol* 2007; **292:** H921–H927.
13. Hasegawa T, Nakatani S, Kanzaki H, Abe H, Kitakaze M. Heterogeneous onset of myocardial relaxation in subendocardial and subepicardial layers assessed with tissue strain imaging: Comparison of normal and hypertrophied myocardium. *J Am Coll Cardiol Img* 2009; **2:** 701–708.
14. Tanimoto T, Imanishi T, Tanaka A, Yamano T, Kitabata H, Takarada S, et al. Bedside assessment of myocardial viability using transmural strain profile in patients with ST-elevation myocardial infarction: Comparison with cardiac magnetic resonance imaging. *J Am Soc Echocardiogr* 2009; **22:** 1015–1021.

15. Reimer KA, Jennings RB. The 'wavefront phenomenon' of myocardial ischemic death. II: Transmural progression of necrosis within the framework of ischemic bed size (myocardium at risk) and collateral flow. *Lab Invest* 1979; **40:** 633–644.
16. Teramoto N, Koshino K, Yokoyama I, Miyagawa S, Ose T, Zeniya T, et al. Experimental pig model of old myocardial infarction with long survival leading to chronic LV dysfunction and remodeling as evaluated by PET. *J Nucl Med* 2011; **52:** 761–768.
17. Sade LE, Severyn DA, Kanzaki H, Dohi K, Gorcsan J 3rd. Second-generation tissue Doppler with angle-corrected color-coed wall displacement for quantitative assessment of regional left ventricular function. *Am J Cardiol* 2003; **92:** 554–560.
18. Hu Q, Wang X, Lee J, Mansoor A, Liu J, Zeng L, et al. Profound bioenergetic abnormalities in peri-infarct myocardial regions. *Am J Physiol Heart Circ Physiol* 2006; **291:** H648–H657.
19. Horiguchi K, Sakakida-Kitagawa S, Sawa Y, Li ZZ, Fukushima N, Shirakura R, et al. Selective chemokine and receptor gene expressions in allografts that develop transplant vasculopathy. *J Heart Lung Transplant* 2002; **21:** 1090–1100.
20. Pagani FD, DerSimonian H, Zawadzka A, Wetzel K, Edge AS, Jacoby DB, et al. Autologous skeletal myoblasts transplanted to ischemia-damaged myocardium in humans: Histological analysis of cell survival and differentiation. *J Am Coll Cardiol* 2003; **41:** 1078–1083.
21. Suzuki K, Murtuza B, Fukushima S, Smolenski RT, Varela-Carver A, Coppen SR, et al. Targeted cell delivery into infarcted rat hearts by retrograde intracoronary infusion: Distribution, dynamics, and influence on cardiac function. *Circulation* 2004; **110:** II225–II230.
22. Toyota E, Matsunaga T, Chilian WM. Myocardial angiogenesis. *Mol Cell Biochem* 2004; **264:** 35–44.
23. Toyota E, Warltier DC, Brock T, Ritman E, Kolz C, O'Malley P, et al. Vascular endothelial growth factor is required for coronary collateral growth in the rat. *Circulation* 2005; **112:** 2108–2113.
24. Risau W. Mechanisms of angiogenesis. *Nature* 1997; **386:** 671–674.
25. Goumans MJ, Valdimarsdottir G, Itoh S, Rosendahl A, Sideras P, ten Dijke P. Balancing the activation state of the endothelium via two distinct TGF-beta type 1 receptors. *EMBO J* 2002; **21:** 1743–1753.
26. Zeng L, Hu Q, Wang X, Mansoor A, Lee J, Feygin J, et al. Bioenergetic and functional consequences of bone marrow-derived multipotent progenitor cell transplantation in hearts with postinfarction left ventricular remodeling. *Circulation* 2007; **115:** 1866–1875.
27. Shweiki D, Itin A, Soffer D, Keshet E. Vascular endothelial growth factor induced by hypoxia may mediate hypoxia-initiated angiogenesis. *Nature* 1992; **359:** 843–845.
28. Nagamatsu T, Fujii T, Kusumi M, Zou L, Yamashita T, Osuga Y, et al. Cytotrophoblasts up-regulate soluble fms-like tyrosine kinase-1 expression under reduce oxygen: An implication for the placental vascular development and the pathology of preeclampsia. *Endocrinology* 2004; **145:** 4838–4845.
29. Munaut C, Lorquet S, Pequeux C, Blacher S, Berndt S, Frankenne F, et al. Hypoxia is responsible for soluble vascular endothelial growth factor receptor-1 (VEGFR-1) but not for soluble endoglin induction in villous trophoblast. *Hum Reprod* 2008; **23:** 1407–1415.
30. Hearse DJ, Maxwell L, Saldanha C, Gravin JB. The myocardial vasculature during ischemia and reperfusion: A target for injury and protection. *J Mol Cell Cardiol* 1993; **25:** 759–800.
31. Panting JR, Gatehouse PD, Yang GZ, Grothues F, Firmin DN, Collins P, et al. Abnormal subendocardial perfusion in cardiac syndrome X detected by cardiovascular magnetic resonance imaging. *N Engl J Med* 2002; **346:** 1948–1953.
32. van Ramshorst J, Atsma DE, Beeres SL, Mollema SA, Ajmone Marsan N, Holman ER, et al. Effect of intramyocardial bone marrow cell injection of left ventricular dyssynchrony and global strain. *Heart* 2009; **95:** 119–124.
33. Buda AJ, Zotz RJ, Gallagher KP. Characterization of the functional border zone around regionally ischemic myocardium using circumferential flow-function maps. *J Am Coll Cardiol* 1986; **8:** 150–158.
34. Homans DC, Asinger R, Elsperger KJ, Erlien D, Sublette E, Mikell F, et al. Regional function and perfusion at the lateral border of ischemic myocardium. *Circulation* 1985; **71:** 1038–1047.
35. Patterson RE, Kirk ES. Analysis of coronary collateral structure, function, and ischemic border zones in pigs. *Am J Physiol Heart Circ Physiol* 1983; **244:** H23–H31.
36. Shudo Y, Matsumiya G, Takeda K, Matsue H, Taniguchi K, Sawa Y. Novel software package for quantifying local circumferential myocardial stress. *Int J Cardiol* 2011; **17:** 134–136.
37. Kainuma S, Taniguchi K, Toda K, Funatsu T, Kondoh H, Nishino M, et al. Restrictive mitral annuloplasty for functional mitral regurgitation. *Circ J* 2011; **75:** 571–579.
38. Takeda K, Matsumiya G, Hamada S, Sakaguchi T, Miyagawa S, Yamauchi T, et al. Left ventricular basal myocardial scarring detected by delayed enhancement magnetic resonance imaging predicts outcomes after surgical therapies for patients with ischemic mitral regurgitation and left ventricular dysfunction. *Circ J* 2011; **75:** 148–156.
39. Saito S, Matsumiya G, Sakaguchi T, Miyagawa S, Yoshikawa Y, Yamauchi T, et al. Risk factor analysis of long-term support with left ventricular assist system. *Circ J* 2010; **74:** 715–722.

STEM CELLS TRANSLATIONAL MEDICINE

TISSUE ENGINEERING AND REGENERATIVE MEDICINE

Bioengineered Myocardium Derived from Induced Pluripotent Stem Cells Improves Cardiac Function and Attenuates Cardiac Remodeling Following Chronic Myocardial Infarction in Rats

KENJI MIKI,[a] HISAZUMI UENAKA,[a] ATSUHIRO SAITO,[b] SHIGERU MIYAGAWA,[a] TAICHI SAKAGUCHI,[a] TAKAHIRO HIGUCHI,[a] TATSUYA SHIMIZU,[c] TERUO OKANO,[c] SHINYA YAMANAKA,[d,e,f,g] YOSHIKI SAWA[a,b]

Key Words. Induced pluripotent stem cells • Bioengineered myocardium • Implantation • Myocardial infarction

[a]Department of Surgery, Division of Cardiovascular Surgery, Osaka University Graduate School of Medicine, Osaka, Japan; [b]Medical Center for Translational Research, Osaka University Hospital, Osaka, Japan; [c]Institute of Advanced Biomedical Engineering and Science, Tokyo Women's Medical University, Tokyo, Japan; [d]Center for iPS Cell Research and Application (CiRA) and [e]Institute for Integrated Cell-Material Sciences, Kyoto University, Kyoto, Japan; [f]Yamanaka iPS Cell Special Project, Japan Science and Technology Agency, Kawaguchi, Japan; [g]Gladstone Institute of Cardiovascular Disease, San Francisco, California, USA

Correspondence: Yoshiki Sawa, M.D., Ph.D., Department of Surgery, Division of Cardiovascular Surgery, Osaka University Graduate School of Medicine, 2-2-E1 Yamada-oka, Suita, Osaka 565-0871, Japan. Telephone: 81-6-6879-3154; Fax: 81-6-6879-3163; e-mail: sawa-p@tissue.med.osaka-u.ac.jp

Received October 12, 2011; accepted for publication April 13, 2012; first published online in SCTM *Express* May 14, 2012.

1066-5099/2012/$20.00/0

http://dx.doi.org/10.5966/sctm.2011-0038

ABSTRACT

Cell-based therapies are promising strategies for myocardial repair following myocardial infarction. Induced pluripotent stem (iPS) cells have the potential to generate many cardiomyocytes, and they hold significant promise for the application of regenerative medicine to heart failure. Here, we developed cardiac tissue sheets, termed bioengineered myocardium (BM), from mouse iPS cells and measured cardiac performance following BM implantation in a rat chronic myocardial infarction model. Immunostaining analyses revealed that the α-actinin$^+$ cell population was isolated with more than 99% purity under specific culture conditions. To evaluate the contribution of BM to the improvements in cardiac performance, we induced myocardial infarction in 30 F344/NJcl-*rnu/rnu* rats by left anterior descending coronary ligation. The rats were randomly divided into two groups, 2 weeks after ligation: a BM implantation group ($n = 15$) and a sham group ($n = 15$). Echocardiography and catheter examination showed that the BM implantation significantly improved cardiac function and attenuated cardiac remodeling compared with the sham group. Histological analyses demonstrated that the implanted BM survived at the epicardial implantation site 4 weeks after implantation. The implanted BM survived and attenuated left ventricular remodeling in the rat chronic myocardial infarction model. Thus, BM derived from iPS cells might be a promising new treatment for heart failure. STEM CELLS TRANSLATIONAL MEDICINE *2012;1:430–437*

INTRODUCTION

Even though remarkable progress has been made in the medical and surgical management of cardiac diseases, heart failure remains a major cause of death worldwide [1, 2]. Cell-based therapies using skeletal myoblasts, bone marrow mononuclear cells, mesenchymal stem cells, and cardiac stem cells were recently introduced for the clinical treatment of ischemic heart disease [3–6]. Bolli et al. [6] reported that intracoronary infusion of autologous cardiac stem cells is effective in improving left ventricular (LV) systolic function and reducing infarct size in patients with heart failure after myocardial infarction (MI). However, other studies [3–5] showed that their effectiveness is limited and that long-term outcomes are unfavorable.

Growth factors secreted from the transplanted cells are thought to improve the damaged myocardium to a certain extent; this occurs via a paracrine effect [7, 8]. Myoblasts or bone marrow mononuclear cells may improve cardiac performance via a paracrine effect, without directly contributing to the improvement of systolic performance by enhancing the contractile ability of the heart [9, 10]. Several researchers have developed certain stem or progenitor cells that can differentiate into cardiomyocytes or generate cardiomyocytes via cell fusion [11, 12], in order to obtain cells that can compensate for lost cardiomyocytes and greatly promote myocardial regeneration in a severely damaged myocardium following transplantation [13, 14]. However, the differentiation rate of these stem or progenitor cells into cardiomyocytes, or their fusion rate, is relatively low. Therefore, improvement of the impaired cardiac performance by these cells is probably mainly due to paracrine effects.

We think that two important issues need to be addressed in order to improve the effectiveness of cell-based therapies for heart failure. First, autologous stem cells, which differentiate into definitive cardiomyocytes at high rates, need to be used to greatly enhance the contractile ability of the myocardium in situations where

large numbers of cardiomyocytes are damaged. Second, these cells need to be delivered to the damaged myocardium at the maximum dose by using sophisticated cell delivery systems. For example, the development of systems that will enable newly generated cardiomyocytes to integrate with each other ex vivo to form cardiac tissue, and enable this cardiac tissue to synchronously contract with the host myocardium following implantation, should be investigated. Such a strategy may provide the best method for regenerating a severely damaged myocardium.

An intelligent cell delivery system, termed cell sheet technology, was recently developed [15–17]. Conventional methods of cell delivery present some disadvantages, such as needle injection, loss of transplanted cells by leakage, poor survival of grafted cells, myocardial damage resulting from injury by the needle and subsequent acute inflammation [18, 19], and the potential to cause a lethal arrhythmia [20]. However, a cell sheet can deliver substantially higher cell numbers to the damaged myocardium than can needle injection, and it can induce significant myocardial regeneration [21]. Pluripotent stem cells have been generated from mouse and human somatic cells by using specific transcription factors (OCT4, SOX2, c-MYC, and KLF4 or OCT4, SOX2, NANOG, and LIN28) [22–24]; cell-based therapy using such induced pluripotent stem (iPS) cells is expected to find widespread clinical applications. There have been several reports on the differentiation of iPS cells into cardiomyocytes [25–27], but it is unknown whether cardiac tissue sheets derived from iPS cells can improve cardiac function in a chronic MI model. In this study, we developed cardiac tissue sheets termed bioengineered myocardium (BM) from mouse iPS cells, and investigated the efficacy of BM derived from iPS cells in a chronic MI model.

Materials and Methods

Cardiac Differentiation of iPS Cells and Purification of iPS Cell-Derived Cardiomyocytes

We cultured and maintained mouse iPS cells (256H18) [28] and embryonic stem (ES) cells (B6G2) on feeder layers of mitomycin-C-treated STO cells (supplemental online data) [22]. For differentiation, 500 iPS cells were resuspended in 30-μl aliquots of differentiation medium (DM; growth medium without leukemia inhibitory factor) and cultured in 96-well HydroCell plates (CellSeed, Tokyo, http://www.cellseed.com) for 2 days. On day 2, an additional 30 μl of DM containing 4 μM 6-bromoindirubin-3′-oxime (BIO; a glycogen synthase kinase-3β inhibitor, to activate the Wnt-signaling pathway) (Calbiochem, San Diego, http://www.emdbiosciences.com) [29] was added to each well. On day 5, the individual embryoid bodies (EBs) obtained were transferred to gelatin-coated 60-mm dishes (200 EBs per dish). The medium was replenished with fresh DM every day. On day 11, the medium was changed to no-glucose Dulbecco's modified Eagle's medium (DMEM) (Invitrogen, Carlsbad, CA, http://www.invitrogen.com) (F. Hattori and K. Fukuda, WO2007/088874; PCT/JP2007/051563, 2007), and the cells were maintained for a further 2–3 days. The medium was then replaced with DM, and on day 15, the cells were used for reverse transcription-polymerase chain reaction (RT-PCR), quantitative RT-PCR, or immunocytochemistry (supplemental online data).

Development of the iPS Cell-Derived Contractile BM

To develop the contracting BM from iPS cells, individual EBs were seeded onto 24-well UpCell plates (CellSeed) (40 EBs per well) on day 5. Each UpCell plate contains cell culture surfaces to which a temperature-responsive polymer, poly(*N*-isopropylacrylamide), is grafted, and from which cells can be detached as a cell sheet simply by reducing the temperature without any enzymatic treatments [15–17].

Next, the medium was changed to DM and no-glucose DMEM as outlined above, until day 15. The iPS cell-derived cardiomyocytes were then detached at room temperature as a cell sheet with a diameter of approximately 10 mm (supplemental online Fig. 1). This cardiac tissue sheet, termed BM, exhibited spontaneous contraction (supplemental online Movie 1) and was used for implantation.

Animal Experiments

We used F344/NJcl-*rnu/rnu* female rats (CLEA Japan, Tokyo, http://www.clea-japan.com) in which MI was induced by left anterior descending (LAD) coronary ligation [21, 30, 31]. Two weeks later, the animals were randomly divided into two groups: the BM implantation group ($n = 15$) and the sham group ($n = 15$) in which we carried out MI surgery, and opened and closed the rat chests 2 weeks later. BM was implanted directly over the scar area without sutures. After detachment from the temperature-responsive dish, the BM was picked up and spread over the surface of the heart, following which it was allowed to attach to the host myocardium for 10–15 minutes. The animal experiments were performed in compliance with the Principles of Laboratory Animal Care formulated by the National Society for Medical Research, and the Guide for the Care and Use of Laboratory Animals prepared by the Institute of Laboratory Animal Resource and published by the National Institutes of Health (NIH Publication No. 86-23, revised 1996). The ethics committee of Osaka University approved all experiments.

Assessment of Cardiac Performance

Echocardiography was performed before implantation and 1, 2, and 4 weeks after implantation. We measured the anterior wall dimension, posterior wall dimension, left ventricular diastolic dimension (LVDd), and left ventricular systolic dimension (LVDs), and then we calculated the LV ejection fraction (EF) and fractional shortening (FS). EF and FS were calculated using the following formulas:

$$EF\ (\%) = [(LVDd^3 - LVDs^3)/LVDd^3] \times 100$$

$$FS\ (\%) = [(LVDd - LVDs)/LVDd] \times 100$$

A catheter examination was performed 4 weeks after implantation; sternotomy was performed using a thin catheter tip, and hemodynamics parameters such as dP/dt (an index that is used clinically to characterize the contractile ability of the heart) maximum (max), dP/dt minimum (min), the time constant of isovolumic relaxation (τ), end-systolic elastance (Ees), and end-diastolic elastance (Eed) were determined.

Preparation of LV Myocardium Specimens for Histological Analysis and RNA Isolation

After performing echocardiography and catheter examination, the hearts ($n = 15$ per group) were removed 4 weeks following

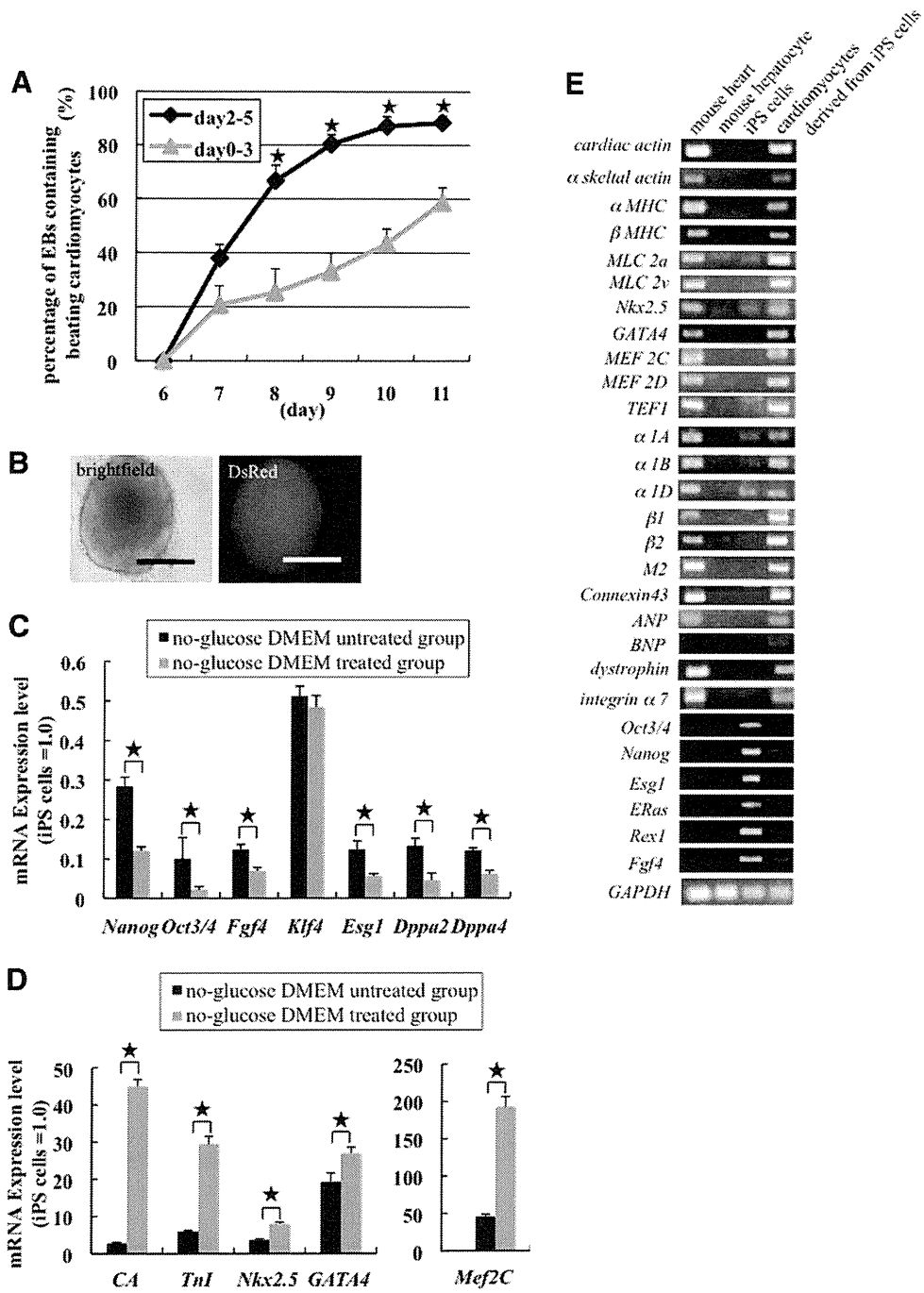

Figure 1. Efficiency of differentiation of mouse iPS cells into cardiomyocytes. **(A):** Number of EBs with beating foci. ⋆, $p < .05$. **(B):** Image of an EB derived from iPS cells obtained on day 5. DsRed was expressed in the EB because the mouse iPS cell line 256H18 was used. Scale bars = 300 μm. **(C–E):** Gene expression in iPS cell-derived cardiomyocytes. Quantitative reverse transcription-polymerase chain reaction (RT-PCR) analyses of the expression levels of undifferentiated cell marker genes (*Nanog*, *Oct3/4*, *Fgf4*, *Esg1*, *Dppa2*, and *Dppa4*) **(C)** and cardiac marker genes (*cardiac actin* [*CA*], *Troponin I* [*TnI*], *Nkx2.5*, *GATA4*, and *Mef2C*) **(D)** in the no-glucose DMEM-treated group and the no-glucose DMEM-untreated group ($n = 5$ per group). ⋆, $p < .05$. **(E):** RT-PCR analyses of cardiac marker genes, such as those for structural proteins (*cardiac actin* to *MLC2v*), transcription factors (*Nkx2.5* to *TEF1*), adrenergic receptors (*α1A* to *β2*), muscarinic receptors (*M2*), other proteins (*connexin 43* to *integrin α7*), and markers for undifferentiated cells (*Oct3/4* to *Fgf4*) in native cardiomyocytes, native hepatocytes, iPS cells, and iPS cell-derived cardiomyocytes. Abbreviations: DMEM, Dulbecco's modified Eagle's medium; DsRed, *Discosoma* red fluorescent protein; iPS, induced pluripotent stem.

implantation and sectioned into two pieces each. Each heart was cut into cross-sections for nine specimens in each group, with one section snap-frozen in liquid nitrogen and two others embedded in O.C.T. compound (Sakura Finetek Japan, Tokyo, http://www.sakura-finetek.com) for immunostaining and Masson's trichrome staining. Fibrosis areas were calculated using MetaMorph Microscopy Automation and Image Analysis Software (Molecular Devices Corp., Union City, CA, http://www.moleculardevices.com). The remaining six specimens in each group were transverse-sectioned; the apex-side specimens were

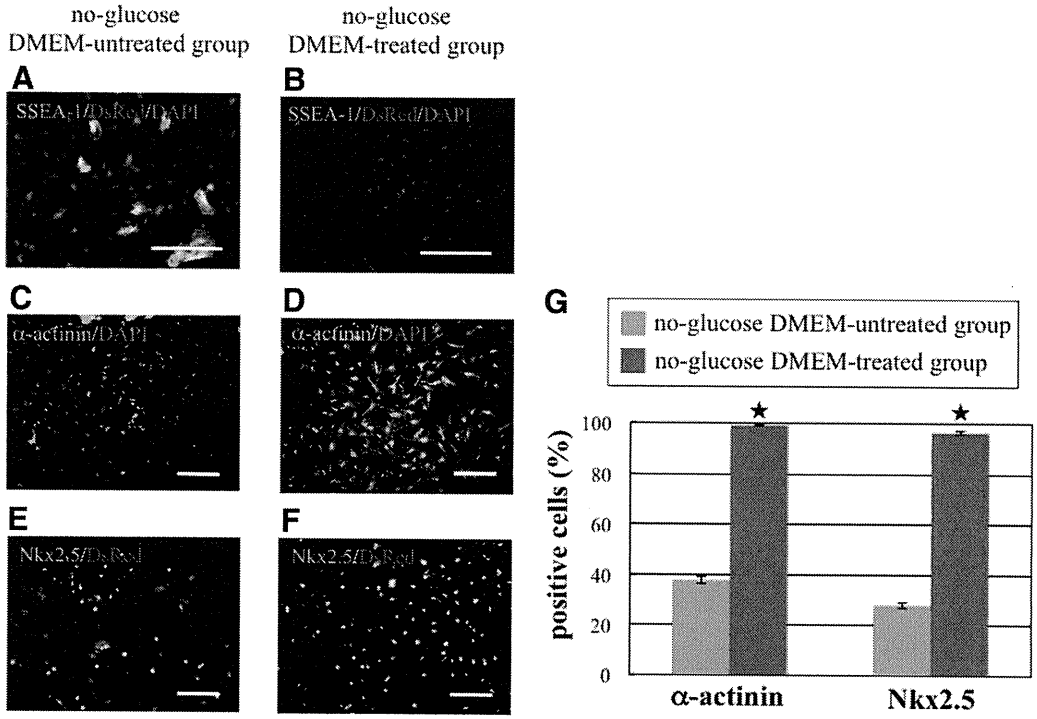

Figure 2. Immunostaining of induced pluripotent stem (iPS) cell-derived cardiomyocytes. **(A–F):** Microscopic images showing differentiated cells on day 15 in the no-glucose DMEM-untreated group **(A, C, E)** and in the no-glucose DMEM-treated group **(B, D, F)**. **(A, B):** Immunostaining of SSEA-1 (green). Nuclei were stained with DAPI (blue); DsRed (red) was expressed in the cytosol of iPS cell-derived cells. Scale bars = 100 μm. **(C, D):** Immunostaining of α-actinin (green). Nuclei were stained with DAPI. Scale bars = 300 μm. **(E, F):** Immunostaining of Nkx2.5 (green) and DsRed (red) expression in the cytosol of iPS cell-derived cells. Scale bars = 300 μm. **(G):** Quantification of α-actinin- and Nkx2.5-positive cells by imaging analysis. In the no-glucose DMEM-untreated group (gray columns), the percentages of α-actinin- and Nkx2.5-positive cells were 37.87% and 27.92%, respectively. In contrast, the percentages of α-actinin- and Nkx2.5-positive cells in the no-glucose DMEM-treated group (red column) were 99.18% and 96.45%, respectively. ⋆, $p < .05$. Abbreviations: DAPI, 4′,6-diamidino-2-phenylindole; DMEM, Dulbecco's modified Eagle's medium; DsRed, *Discosoma* red fluorescent protein; SSEA, stage-specific embryonic antigen.

dissected to remove the right ventricular free wall and divided into two pieces from either the infarction or the remote sites. Each specimen was stored in RNAlater solution (Qiagen, Hilden, Germany, http://www1.qiagen.com) for RNA isolation and in T-PER Tissue Protein Extraction Reagent (Thermo Fisher Scientific, Waltham, MA, http://www.thermofisher.com) for the enzyme-linked immunosorbent assay (ELISA) (supplemental online data).

Statistical Analysis

All values are expressed as mean (SD). Statistical comparison of the data was performed using unpaired two-sided *t* tests. A *p* value of <.05 was considered statistically significant.

Results

Expression of Several Cardiac Markers by iPS Cell-Derived Cardiomyocytes and Procurement of α-Actinin-Positive Cardiomyocytes with More than 99% Purity

To obtain high-purity cardiomyocytes from iPS cells (256H18 clone), we first generated EBs by treatment with BIO and determined the best culture conditions to induce the differentiation of iPS cells into cardiomyocytes. When EBs were cultured with BIO from day 2 until day 5, spontaneous contraction occurred within the small foci in approximately 88% of the EBs on day 11. In contrast, when EBs were cultured with BIO from day 0 until day 3, the number of beating foci significantly decreased from day 8 to day 11 when compared with the cells cultured with BIO from day 2 to day 5 (Fig. 1A). The EBs formed from the 256H18 iPS cell line expressed *Discosoma* red fluorescent protein (DsRed) in the cytosol (Fig. 1B). When EBs derived from ES cells were treated with BIO on days 2–5, they exhibited spontaneous contraction equivalent to that of the iPS cells treated with BIO for the same period (supplemental online Movie 2).

In order to avoid teratoma formation after implantation, we changed the DM to no-glucose DMEM for days 11–12 or 13, and then reverted to DM the next day. This method enabled us to easily select differentiated cardiomyocytes from undifferentiated cells based on their different energy consumption requirements.

We performed RT-PCR, quantitative RT-PCR, and immunostaining with differentiated cells from day 15 to investigate the purification efficiency. Quantitative RT-PCR analysis revealed that the expression of undifferentiated cell marker genes (*Nanog*, *Oct3/4*, *Fgf4*, *Esg1*, *Dppa2*, and *Dppa4*) was significantly lower in the no-glucose DMEM-treated group than in the no-glucose DMEM-untreated group. These data indicated that iPS cells cultured in no-glucose DMEM had lower potential to form tumors following implantation (Fig. 1C). The expression of cardiac marker genes (*cardiac actin*, *TnI*, *Nkx2.5*, *Gata4*, and *Mef2C*) was significantly higher in the no-glucose DMEM-treated group than in the no-glucose DMEM-untreated group (Fig. 1D). Therefore, we surmised that no-glucose DMEM treatment significantly increases the purity of differentiated iPS cell-derived cardiomyocytes by destroying noncardiomyocytes. RT-PCR analysis further revealed that iPS cell-derived cardiomyocytes treated with BIO and no-glucose DMEM expressed several cardiac markers,

such as structural proteins, transcription factors, adrenergic and muscarinic receptors, and connexin 43, to nearly the same extent as the native cardiomyocytes did (Fig. 1E). Conversely, markers (*Oct3/4*, *Nanog*, *Esg1*, *Eras*, *Rex1*, and *Fgf4*) for undifferentiated cells were downregulated in iPS cell-derived cardiomyocytes compared with iPS cells (Fig. 1E). Immunostaining of stage-specific embryonic antigen-1 (SSEA-1) (a marker of undifferentiated cells) revealed that a few SSEA-1-positive cells remained alive in the no-glucose DMEM-untreated group even at day 15, but that SSEA-1-positive cells were observed in the no-glucose DMEM-treated group (Fig. 2A, 2B). In contrast, immunostaining of α-actinin and Nkx2.5 (cardiac markers) revealed that the percentages of α-actinin and Nkx2.5-positive cells in the no-glucose DMEM-untreated group were 37.87% and 27.92%, respectively, but those in the no-glucose DMEM-treated group were 99.18% and 96.45%, respectively (Fig. 2C–2G). Thus, we successfully obtained high-purity cardiomyocytes from iPS cells by using the combined BIO and no-glucose DMEM culture methods.

Improvement in Cardiac Performance and Attenuation of Remodeling by the BM Derived from iPS Cells

We next investigated the therapeutic effect of the BM derived from iPS cells in vivo by inducing MI in F344/NJcl-*rnu/rnu* rats (nude rats) and then implanting the BM derived from iPS cells onto the infarcted area 2 weeks after the infarction. Echocardiographic analysis revealed that FS improved and LVDd decreased in the group implanted with the BM derived from iPS cells (i.e., the BM group) 4 weeks following implantation (Fig. 3A, 3B; supplemental online Table 1). Thus, the BM improved systolic performance and attenuated LV dilatation. The systolic and diastolic performances also improved after implantation, as revealed by pressure-volume analysis (Fig. 3C). The hemodynamics indices were then determined by performing a catheter examination. Significantly higher Ees and lower Eed, higher dP/dt max and lower dP/dt min, and lower τ were observed in the BM group compared with the sham group 4 weeks after implantation (Fig. 4A, 4B). Thus, these parameters indicate that the BM derived from iPS cells improved systolic and diastolic performances.

Survival and Attenuation of Fibrosis by the BM Derived from iPS Cells at the Epicardial Implantation Site 4 Weeks After Implantation

We obtained LV myocardial specimens 4 weeks after implantation to confirm the survival of the implanted BM derived from iPS cells. Masson's trichrome staining revealed less fibrosis and increased thickness of the anterior wall at the site where the BM was implanted (Fig. 5A, 5B, 5E, 5F). Fluorescence microscopy revealed that the implanted BM, which expressed DsRed in the cytosol, survived at the epicardial implantation site (Fig. 5C, 5D, 5G, 5H). Immunohistochemistry revealed that DsRed-positive surviving cells expressed α-actinin in the sarcomere (Fig. 5I–5N). In addition, the percentage of fibrosis in the BM group was significantly lower than that in the sham group (supplemental online Fig. 2). Furthermore, ELISAs performed for hepatocyte growth factor (HGF) and vascular endothelial growth factor (VEGF) revealed that the expression levels of these angiogenic proteins were higher in the BM group than in the sham group (supplemental online Fig. 3). These data indicated that the BM derived from iPS cells also induced a paracrine or autocrine effect by secreting angiogenic factors and inducing angiogenesis in the impaired myocardium. Thus, these data indicate that the BM derived from iPS cells may improve cardiac performance in severely damaged myocardium by directly affecting contractile function and inducing a paracrine effect on angiogenic proteins.

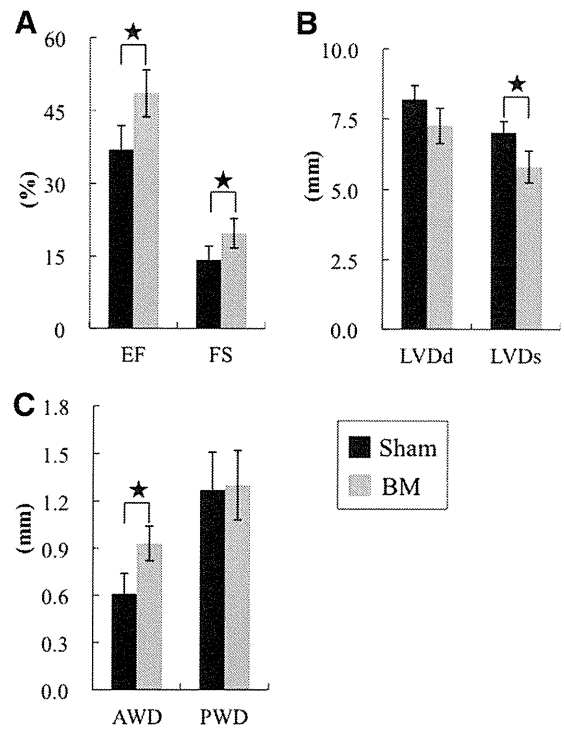

Figure 3. Effects of the induced pluripotent stem cell-derived BM on postinfarct ventricular function at 4 weeks by echocardiography. Shown is echocardiographic assessment of EF **(A)** (left) and FS **(A)** (right), LVDd **(B)** (left), LVDs **(B)** (right), AWD **(C)** (left), and PWD **(C)** (right) in the BM group ($n = 15$) and the sham group ($n = 15$). ★, $p < .05$. The systolic performance was significantly improved and the left ventricular dilatation was attenuated in the BM group compared with the sham group. Abbreviations: AWD, anterior wall dimension; BM, bioengineered myocardium; EF, ejection fraction; FS, fractional shortening; LVDd, left ventricular diastolic dimension; LVDs, left ventricular systolic dimension; PWD, posterior wall dimension.

Discussion

We previously demonstrated that neonatal cardiomyocyte sheets can survive in the hearts of rats with chronic MI and that cardiac performance was improved by the successful electrical and histological integration of these sheets into the host myocardium [30]. However, this strategy cannot be used in clinical settings because the large numbers of neonatal cardiomyocytes required cannot be obtained under ethical guidelines. Therefore, we attempted to use autologous iPS cells, due to their high cardiomyocyte differentiation rates. Such cells may completely regenerate a damaged myocardium and contribute to the armamentarium of heart failure management in clinical settings.

Our data indicate that the iPS cell-derived cardiomyocytes, differentiated by combined treatment with BIO and no-glucose DMEM, expressed cardiac markers and were highly similar to native mouse cardiomyocytes. As seen in supplemental online Figure 4, the organization of α-actinin in iPS cell-derived cardiomyocytes was random and similar to that of mouse neonatal cardiomyocytes. We postulate that the iPS cell-derived cardiomyocytes generated using our protocol included embryonic- and adult-phenotype ventricular and atrial myocytes.

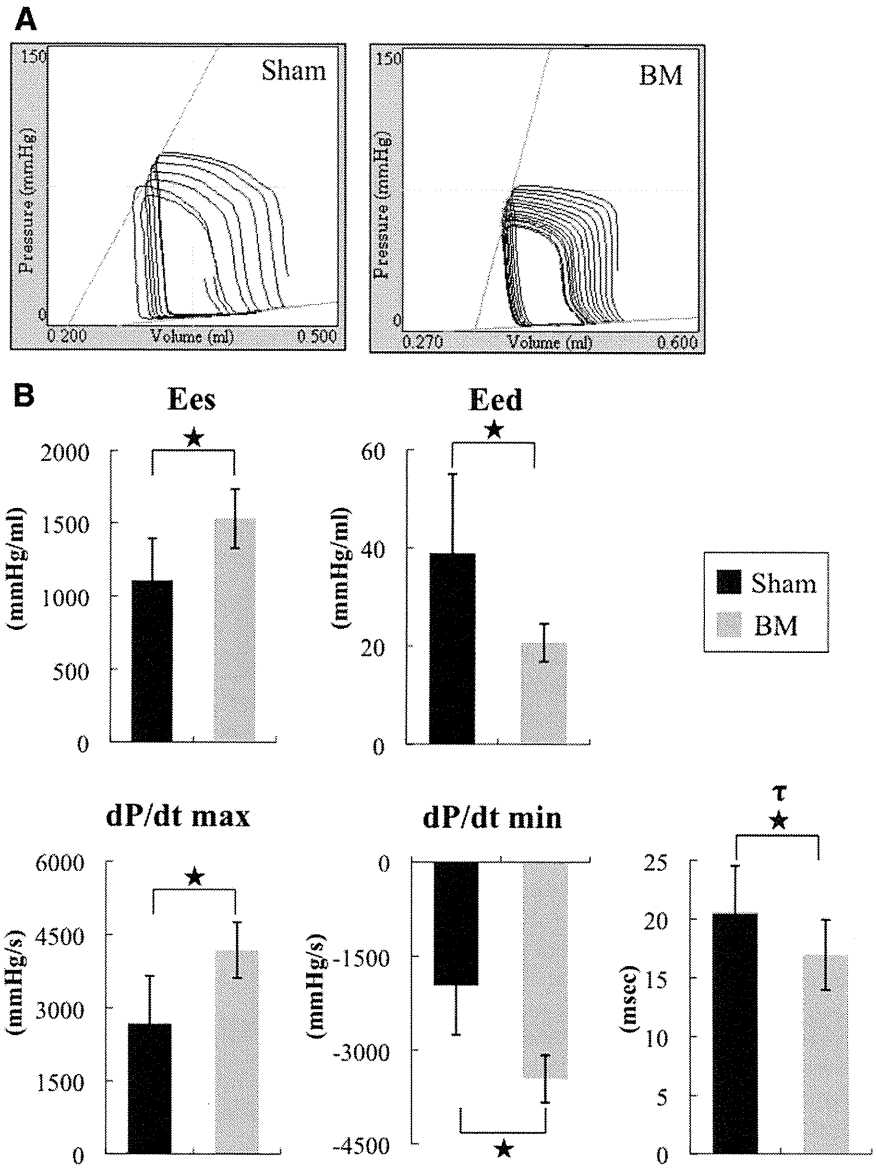

Figure 4. Effects of the induced pluripotent stem cell-derived BM on postinfarct ventricular function at 4 weeks by catheter examination. **(A):** Representative pressure-volume loops of the sham and BM groups. The systolic and diastolic performances of the BM group were significantly better than those of the sham group. **(B):** Catheter examination of Ees, Eed, dP/dt max, lower dP/dt min, and lower τ in the BM group ($n = 15$) and the sham group ($n = 15$). ★, $p < .05$. Abbreviations: BM, bioengineered myocardium; Eed, end-diastolic elastance; Ees, end-systolic elastance; max, maximum; min, minimum.

The most significant finding of the present study is the ability of the iPS cell-derived BM to improve cardiac performance, attenuate cardiac remodeling, recover wall thickness, and survive at the epicardial implantation site after implantation. These findings led us to explore the mechanism by which this improvement occurs. We believe that this improvement is achieved by two effects: (a) a direct effect of the BM synchronously contracting with the host myocardium, and (b) a paracrine effect of growth factors secreted at the site of implantation. We have previously demonstrated that (noncontracting) fibroblast sheets failed to improve systolic performance compared with neonatal cardiomyocyte sheets, and we did not observe recovery of wall thickness in the fibroblast sheet-implantation group [30]. In this study, the implanted contracting BM improved cardiac performance, recovered wall thickness, and survived at the epicardial implantation site for up to 4 weeks after implantation. This suggests that the BM, similar to neonatal cardiomyocyte sheets [30], synchronously contracts with the host myocardium and directly improves systolic performance. However, as seen in Figure 5M and 5N, DsRed-negative cells were observed in the BM on magnification images. We speculate the following explanation. In the previous study [30], we showed that host cells such as fibroblasts, endothelial cells, and some stem cells migrate into the transplanted sheet in response to HGF and VEGF. Therefore, host cells may similarly migrate into the BM. Moreover, we did not dissociate cardiomyocytes before implantation of the BM, because this destroys the extracellular matrix and gap junctions. As seen in Figure 2D, almost all of the surviving cells in no-glucose DMEM were α-actinin$^+$ cells. However, once the cardiomyocytes are dissociated, they do not reconstruct a sheet even if high-purity cardiomyocytes are seeded at a high density onto UpCell. Then, in this study, to obtain the BM as a sheet, we did